OXIDATIVE BEHAVIOR AND THERMAL STABILITY OF C_{60} COLLOIDAL SUSPENSIONS IN WATER AND C_{60}/γ-CYCLODEXTRIN POLYMER NETWORKS

By

RANGIKA S. HIKKADUWA KORALEGE

Bachelor of Science in Chemistry
University of Kelaniya
Kelaniya, Sri Lanka
2007

Submitted to the Faculty of the
Graduate College of the
Oklahoma State University
in partial fulfillment of
the requirements for
the Degree of
DOCTOR OF PHILOSOPHY
December, 2014

OXIDATIVE BEHAVIOR AND THERMAL STABILITY OF C_{60} COLLOIDAL SUSPENSIONS IN WATER AND C_{60}/γ-CYCLODEXTRIN POLYMER NETWORKS

Dissertation Approved:

Dr. Kevin D. Ausman

Dissertation Adviser

Dr. Frank D. Blum

Dr. Jeffery L. White

Dr. Kenneth D. Berlin

Dr. Carey N. Pope

Outside Committee Member

ACKNOWLEDGEMENTS

I would like to express my sincere gratitude to Dr. Kevin D. Ausman for his advice and encouragement during my years at Oklahoma State University, without whom none of this would have been possible. His unending patience and his ideals are, and shall continue to be, my inspiration.

I would like to thank all who served on my advisory committee: Dr. Kevin D. Ausman (Advisor/Chair), Dr. Frank D. Blum, Dr. Jeffry L. White, Dr. Kenneth D. Berlin and in addition to Dr. Carey N. Pope who served as my outside member (Department of Physiological Sciences) for their guidance and support. Special thanks to Dr. Asfaha Iob, Dr. David Jocobs and Dr. Loralee Ohrtman for their assistance with shared instrumentation, helpful discussions and borrowed chemicals and supplies. Also, I would like to thank Oklahoma State University Chemistry Department for their support and guidance during my stay at Oklahoma State University.

My special thanks go out to my predecessors, Befrika Murdianti, Martha Hilburn and Randall Maples for laying the groundwork for these studies, helpful discussions, teamwork and continuous support. Also, I would like to thank my collaborators, Dr. Jeffery L. White, Dr. Gaumani Gyanwali and Mathis Hodge for their useful insights and teamwork.

I received tremendous support and encouragement from my family. My parents and my sister have provided unending support for my career choice, without whom I would not be where I am today. My son Vinuka has become the essence of my hopes for the future. And for Nuwan, there aren't enough words, you helped me develop my ideas and supported me through every hardship. Thank you for everything.

Finally, I would like to gratefully acknowledge funding for this work from an Oklahoma State Regents for Higher Education grant, Oklahoma State University, National Science Foundation and the Gilbert and Nancy Williams Chemistry Graduate Fund.

Name: RANGIKA S. HIKKADUWA KORALEGE

Date of Degree: DECEMBER, 2014

Title of Study: OXIDATIVE BEHAVIOR AND THERMAL STABILITY OF C_{60} COLLOIDAL SUSPENSIONS IN WATER AND C_{60}/γ-CYCLODEXTRIN POLYMER NETWORKS

Major Field: CHEMISTRY

Abstract:

Since its discovery in 1985, buckminsterfullerene (C_{60}) has been extensively studied due to its unique properties and it's now being produced in multi-ton quantities. The ability to form stable aqueous C_{60} colloids (known as nano-C_{60} or *n*C_{60}) and the availability of these in natural systems at environmentally-relevant concentrations led to significant interest concerning the environmental health and safety of these colloidal aggregates. Addressing two issues with regard to this material's environmental health and safety concerns we have looked at the oxidative mechanism of these *n*C_{60} colloidal aggregates and their thermal stability. For making accurate kinetics and measurements on oxidation caused by aqueous-*n*C_{60} colloidal dispersions, we have developed experimental methods utilizing dihydrorhodamine 123 (DHR123) as a sacrificial probe molecule to monitor oxidation by fluorescence spectroscopy and kinetic models to explain observed oxidation. Evaluation of the oxidative behavior of fullerene colloids has been determined using the oxidation rate as a function of *n*C_{60} concentration, *n*C_{60} surface area, number of colloidal particles and $C_{60}O$ content, operating where necessary under inert atmosphere and oxygen rich conditions. The effect of temperature on these colloids plays a significant role in both their synthesis and reactivity. Given that the colloids are mainly composed of C_{60} and $C_{60}O$, $C_{60}O$ might play a significant role in stabilizing the colloid, hence increasing the temperature might cause thermally-activated reactions with $C_{60}O$. Thermal stability of these colloids prepared by all four primary *n*C_{60} synthesis methods has been investigated. Incorporation of C_{60} into polymers is of potential interest for applications, for sequestration to address potential environmental health and safety issues, and as a component in novel architectures. A new composite material was developed by encapsulating C_{60} into cross-linked polymer network formed by γ-cyclodextrin. A simple synthesis route to achieve composite membranes of intercalated C_{60} in the polymer network is presented.

TABLE OF CONTENTS

Chapter Page

LIST OF TABLES

LIST OF FIGURES

Figure Page

Figure Page

Figure Page

CHAPTER I

INTRODUCTION

1.1 Background

The possibility of the existence of buckminsterfullerene (*a.k.a.*, fullerene) was first predicted by a Japanese chemist Eiji Osawa from Toyahashi University of Technology in 1970.[1] He observed that the structure of a corannulene molecule was a subset of a soccer-ball shape structure, and he made the hypothesis that a full ball shape could also exist. Later, in 1981 R. A. Davidson used graph theory to deduce an algebraic solution of the Hückel calculations for fullerene[2] and in year 1985, A. D. J. Haymet published his studies on the Archimedean solids; footballene (C_{60}) and archimedene (C_{120}).[3] In 1996, Richard E. Smalley and Robert F. Curl from Rice University and Sir Harold W. Kroto from the University of Sussex were awarded the Nobel Prize in Chemistry for the discovery of the hollow-sphere fullerene, termed as buckminsterfullerene or fullerene (C_{60}) in 1985.[4, 5] The name fullerene was derived from R. Buckminster Fuller's geodesic architectural structures that resemble the proposed shape of the fullerene molecule. Fullerenes are truncated icosahedrons and C_{60} is a polygon with 60 vertices and 32 faces, 12 of which are pentagonal and 20 hexagonal. Each carbon atom is covalently bonded to three carbon atoms forming conjugated double bonds. There are two distinct C=C

bonds present in fullerene, the [6,6]- and the [5,6]- bonds, where [6,6]- bonds can be found at the edge between two hexagons and the [5,6]- bonds are between hexagons and pentagons as shown in Figure 1.1.

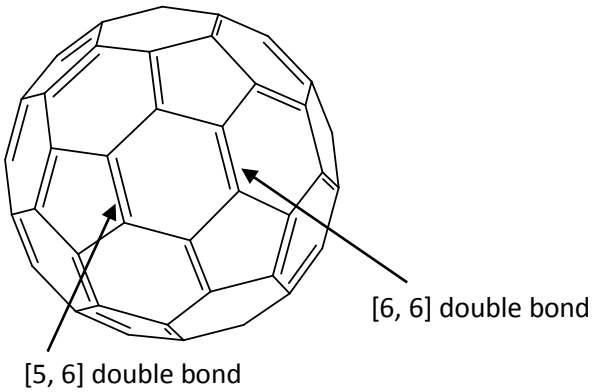

Figure 1.1 Structure of fullerene C_{60}

Fullerenes were synthesized from pure graphitic carbon soot, by evaporating graphite electrodes in an atmosphere of ~100 torr of helium, and were first produced in bulk quantities by Kratschmer *et al*. in 1990.[6] Due to continuing progress of nanotechnology and extensive research concerning potential applications of fullerenes, it is now being synthesized in multi-ton quantities by Frontier Carbon Corporation (FCC) located Kyushu in Japan.[7] As a result of this increased production of fullerenes, usage, and potential release of these materials to environment increased accordingly leading to concern about increased human and environmental exposure. Regardless of the ultimate commercial significance of these materials, contradictory claims about their properties have led to significant concerns regarding their biological and environmental impacts, raising C_{60} to a touchstone nanoparticle throughout the scientific community with respect to biological and environmental interactions.

C_{60} is known to have a very low solubility in water, $<10^{-9}$ mg/L.[8] This low solubility, however, does not reflect the larger issue of water availability. C_{60} has a tendency to form stable colloidal aggregates (nano-C_{60} or *n*C_{60}) in most aqueous conditions, making the *n*C_{60} form to be a vital starting point and a fundamental model for comparing all fullerene impact studies.[9-11]

Fullerene colloidal aggregates can be synthesized by either long-term stirring of C_{60} powder in water (AQU method)[10] or by solvent exchange methods such known as THF, TTA, SON and HIPA [9, 10, 12-14]. The THF method was developed by Deguchi[15] and it involves the mixing of C_{60} in tertrahydrofuran (THF) followed by addition of water to the mixture and evaporation of the organic solvent by rotary evaporation. The rate of addition of water determines the resulting *n*C_{60} particle size. The TTA method was developed by Scrivens[13] and "TTA" is an abbreviation referring to the successive solvents used in the method: toluene, tetrahydrofuran, and acetone. This method attempts a gradual transition from a "good" solvent (toluene) to a "poor" solvent (water) through intermediate solvents (tetrahydrofuran and acetone). This method also gives controlled particle growth and a narrow range of particle sizes.[12, 13] The sonication method (abbreviation SON) was first proposed by Andrievsky[9]. In this method ultrasonication is used to facilitate the transfer of C_{60} from toluene to water. The SON method gives rise to extremely high colloidal concentrations compared to other literature methods. Regardless of these high concentrations, the SON method has the least controlled conditions due to the locally-violent conditions ultrasonication provides, leading to variable colloidal particle sizes and wide range of side reactions with the fullerene cage. The HIPA method was developed by Hilburn[14] in 2012 where "HIPA" is an abbreviation referring to the solvents used: hexane and isopropyl alcohol. This approach is quite similar to the TTA method as it uses gradual transition of C_{60} from a "good" solvent (hexane) to a "poor" solvent (water), but unlike the TTA method, HIPA use solvents that decrease in C_{60} solubility along with decrease in vapor pressure which allows solvents to be removed in the same order in which they were added. Finally, the AQU method[10, 12] involves long term stirring of C_{60} powder in water for a period of days to months, thereby avoiding the use of any organic solvents. This method results in low colloidal concentrations and little control over the particle size range.

Apart from the synthesis methods discussed above which began with pristine C_{60} powder, C_{60} can be chemically modified deliberately to render it water soluble. Sayes *et al.*[16] have described a range of possible derivatizations that have been made to the pristine cage of C_{60} via covalent bonding that resulted in varying levels of water solubility (13000-100000 mg/L).[16-22] One example of such modification is functionalization of the C_{60} cage with hydroxyl groups to produce fullerol, which consist of, on average 14-15 hydroxy groups.[23] Torres *et al*[24] have investigated the solubilization of fullerenes using different solubility enhancers such as surfactants (Triton X-100, Tween-20. 60 & 80, sodiumdodecyl sulphate) and polymer solubilizers (polyoxyethylene & polyvynilepyrrolidine).

1.2 Stability of C_{60} colloidal suspensions

The ability of suspended colloidal particles to resist aggregation for an indefinite period of time is true for an excellent colloidal suspension, where aggregation refers to the association of colloidal particles to form larger clusters. The unusual colloidal stability shown by supposedly hydrophobic C_{60} nanoparticles has been highlighted in several studies.[9, 13, 15, 25, 26] $n$$C_{60}$ made via the SON method has shown high stability with no essential changes being observed on storing in the absence of light at low temperature for three months. These suspensions showed little reverse extraction by toluene, were stable in the pH range 1-10, and were unaffected by boiling.[9] Brant *et al.*[27] has shown evidence that the $n$$C_{60}$ clusters made by THF/$n$$C_{60}$ method remained relatively stable under quiescent conditions and showed little propensity to aggregate. In another study Brant[28] has reported that THF/$n$$C_{60}$ and AQU/$n$$C_{60}$ suspensions remained stable for several months at low ionic strengths, and that aggregation increased with increasing ionic strengths of

the solutions. Deguchi[15] has reported that the THF/$n$$C_{60}$ suspensions were very stable and no precipitation occurred even after 9 months of storage in the dark at room temperature.

Some researches described the unusual stability of C_{60} colloids[9, 27] has been achieved through formation of a donor-acceptor complex with water and possibly responsible for the surface charge that stabilizes the colloids.[9, 11, 15, 29] Labille[30] has reported that the stabilization of $n$$C_{60}$ dispersions happens via hydration of the C_{60} surface which leads to the formation of hydroxylated species at the surface. However, more recent findings by Murdianti[31] demonstrated that stability of aqueous fullerene colloidal suspensions relies on [6,6]-closed epoxide derivative of the fullerene ($C_{60}O$).

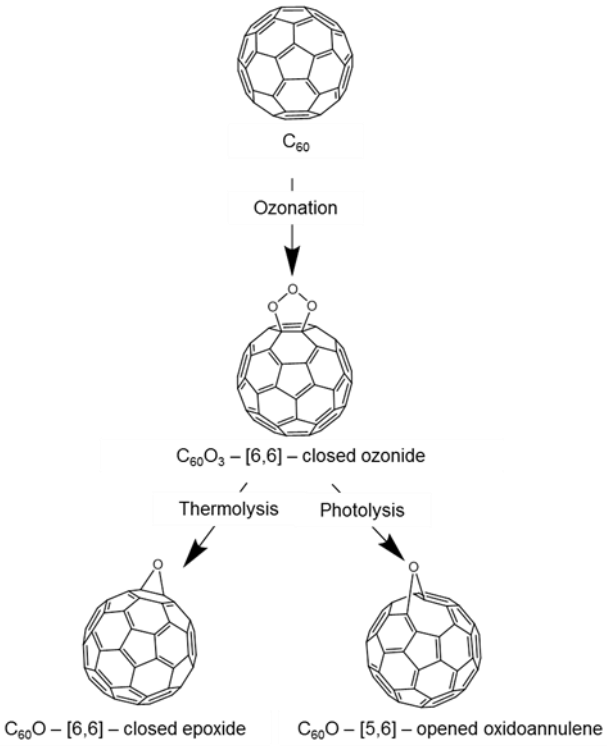

Figure 1.2 Reaction pathways for the formation of $C_{60}O$ isomers

$C_{60}O$ can also be formed by solution phase ozonation of C_{60}, which generates ozonides to give either epoxide or oxidoannuelne upon further dissociation via thermolysis and photolysis, respectively, as shown in Figure 1.2.[32, 33] In uncontrolled conditions, the reaction with ozone can

also yield higher oxides such as $C_{60}O_n$ where n>1 as shown in the HPLC chromatogram Figure 1.3 below.

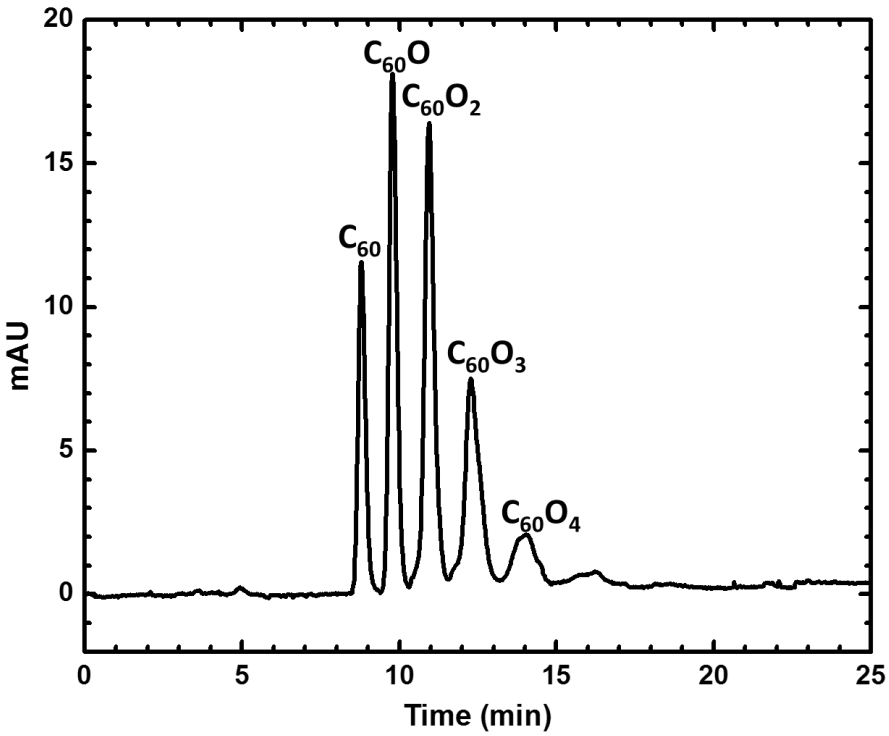

Figure 1.3 HPLC chromatogram showing the reaction of C_{60} with ozone producing higher oxides of fullerene

According to Murdianti[31] enriching C_{60} solids with epoxide isomer of $C_{60}O$ resulted in a significantly accelerated formation of the colloidal particles even under an inert atmosphere. Further experimentation and *n*C_{60} synthesis under different conditions have confirmed that the epoxides present on the colloid surface as shown in Figure 1.4, is accountable for the stability of AQU/*n*C_{60} suspensions.

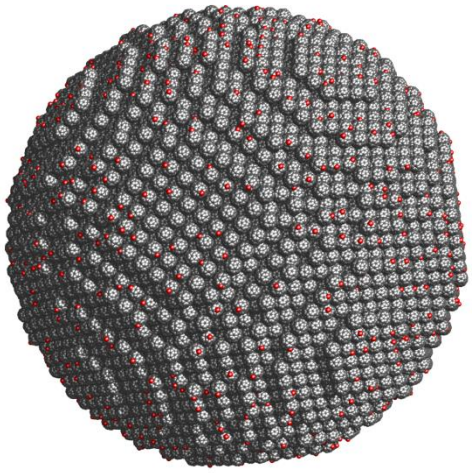

Figure 1.4 *n*C_{60} colloidal particle with 41% surface coverage of $C_{60}O$ (oxygen atoms shown in red)

1.3 Toxicity controversies and oxidative behavior of nC_{60}

The first report on cytotoxicity of fullerene colloidal suspensions on human cell cultures was published by a team of scientists from Rice University and Georgia Institute of Technology in 2004.[16] They have observed oxidative damage to the cell membranes of human dermal fibroblasts (HDF) and human liver carcinoma cells (HepG2) in-vitro where fullerene exposure led to cell death. It was concluded that under ambient conditions in water fullerenes can generate superoxide anions and these oxygen radicals were responsible for membrane damage and subsequent cell death. They also reported that highly water-soluble functional groups on the surface, such as hydroxyl groups, of a fullerene molecule dramatically decreased the toxicity of pristine C_{60}. Another study by Sayes[34] in 2005, further confirmed that *n*C_{60} demonstrated significant toxicity in cell culture studies, where lipid peroxidation and resultant membrane

damage were responsible for the cytotoxicity. The capability of nano-C_{60} to generate superoxide anions in cell free conditions[16] was evident and suggested that nano-C_{60} itself being the origin of the oxygen radicles, and hence acting as a pro-oxidant.[34] Another study by Oberdorster[35] has highlighted that significant lipid peroxidation was observed in brains of largemouth bass after exposure to *n*C_{60} compared to controls. She postulated that in lipid-rich regions of the brain, the colloid dissociated and freed individual redox-active fullerenes or a reactive fullerene metabolite was formed. Following these observations, there were numerous reports on cytotoxicity of *n*C_{60} which supported its pro-oxidant behavior. According to Isakovic[36] *n*C_{60} was at least 3 orders of magnitude more potent in cytotoxicity assays with mouse fibrosarcoma cells, rat glioma cells and human glioma cells, than polyhydroxylated fullerenes ($C_{60}(OH)_n$). Authors have provided clear evidence of *n*C_{60} being a pro-oxidant in contrast to its hydroxylated derivative which showed an antioxidant behavior in cell culture studies and consequently the mechanisms underlying pro-oxidant versus antioxidant behaviors were accounted for big structural differences.

In contrast to these findings, which confirmed that the observed cytotoxicity was primarily due to oxidative damage, evidence began to accumulate contradicting the oxidative toxicity potential for *n*C_{60}.[37-41] According to Lyon *et al*[37], *n*C_{60} was not responsible for any ROS production or ROS-mediated damage in *E. coli* and *B. subtilis* bacteria, thus hypothesizing *n*C_{60} was involved in an ROS-independent oxidative stress. They have also reported that ROS-mediated damage was interfered by *n*C_{60}. Leading to false positives, it was proposed that direct oxidation of the dyes by *n*C_{60} have been confused with *n*C_{60}'s toxicity via ROS-production. Andrievsky[38] has reported that the hydrated fullerenes (HyFn) are incapable of producing strong oxidants such as ROS, superoxide radical, singlet oxygen, etc. due to the hydrated shells present on the surface of C_{60} as described by his HyFn model. According to his explanation, the hydrated shells will avoid molecular oxygen being in contact with C_{60}, and hence, he suggested a long-term anti-oxidative activity shown by hydrated fullerenes was due to the presence of highly ordered

water shells surrounding C_{60}. Another study by Gharbi[39] demonstrated the capability of C_{60} to protect rat liver cells against CCl_4 acute toxicity in a dose dependent manner by modulating the oxidative stress. He further supported the idea of C_{60} being a powerful liver-protective agent, hence an anti-oxidant, by histopathological examinations and biological tests. C_{60}'s protection effect on lipid peroxidation has also being reported by Wang[42] and showed that the anti-oxidant activity is even greater than that of vitamin-E.

Traditionally oxidative damage in biological systems has being described as occurring through ROS mediated peroxidation, due to the presence of an oxidant which in turn creates ROS that are long-liv ed enough to cause damage to the cells. Consequently assays to measure ROS production in cells has become a norm in biological community to account for oxidative damage. As described in the text above, the apparent contradictions in the *n*C_{60} literature can be reconciled by scrutinizing the initially published reports on measurement of cytotoxicity ensued by fullerene colloids (*n*C_{60}) as a result of direct oxidative damage, and therefore claimed an oxidative damage mechanism.[34-36] Others reported a marked lack of oxidation or in some cases anti-oxidant activity were in fact measuring the oxidation that occurs due to reactive oxygen species (ROS).[37, 39]

Apart from these contradictions of direct oxidation versus anti-oxidant activity, some later reports attributed the oxidation happening in these fullerene suspensions was completely due to contaminants present in fullerene colloidal suspensions such as decomposition products of tetrahydrofuran as a result of the synthesis procedures utilized.[36, 38-41, 43-45] Moreover, Andrievsky[38] claimed that *n*C_{60} produced, via solvent exchange methods such as THF method, N-methyl-pyrrolidone (NMP) method or other polar solvents, should not be used for biological studies for to many reasons, including irreproducibility of composition of dispersed particles, as well as particle size distribution and contaminations from both organic solvents and other impurities which could ultimately affect the true biological properties of pristine C_{60}. The first report that linked toxic effects directly to a tetrahydrofuran degradation product, γ-butyrolactone

rather than to *n*C_{60} was published by Henry *et al.* in 2007.[44] He claimed that the toxic effects due to THF or THF degradation products cannot be excluded from previous research by Lovern[46], Oberdorster[35] and Sayes[16] who utilized THF/*n*C_{60} suspensions. γ-Butyrolactone was found to be acutely toxic at low concentrations, and THF/*n*C_{60} was more toxic than THF/water based on larval zebrafish survival and gene expression patterns due to higher concentrations of γ-butyrolactone found in THF/C_{60}. This study also suggested that the presence of C_{60} perhaps enhanced the production of γ-butyrolactone. Following Henry's report, in 2009 Sphon[47] reported his findings on biological effects of THF/*n*C_{60} compared to water-stirred C_{60} fullerene suspensions on *Daphnia magna* and the human lung epithelial cell line. THF/*n*C_{60} has shown 3.5-fold increase in ROS production compared to water-stirred C_{60}. THF directly applied to the human lung epithelial cells did not induce ROS formation in a concentration range of 100-1600 ppm. This was a confirmation that THF itself was not responsible for the damage. Futhermore, THF/*n*C_{60} hasn't shown any toxic effect to D. magna and human lung cells when side products were eliminated by additional washing steps which suggested that the possible toxic side products were washed out during washing steps. This observation was further confirmed by using the first wash water fraction, and it was able to double the level of ROS compared to untreated cells, and thus indicating that the possible toxic side product was transferred to the wash water. Sphon, *et al.*, has also described a possible scheme of THF producing side reaction. THF is known to be easily oxidized to form the first intermediate which is a highly reactive THF hydroperoxide, a well-described oxidation product of THF,[48, 49] which then is homolytically cleaved to produce γ-butyrolactone and water, as shown in Figure 1.5.[47]

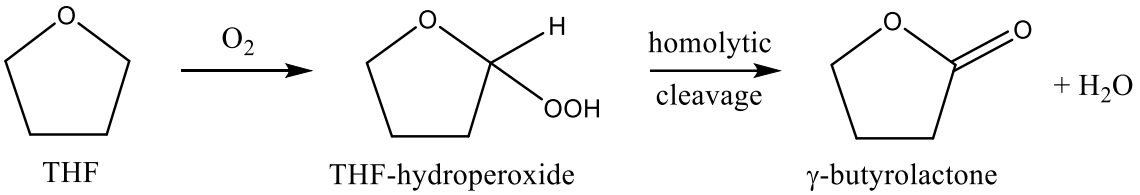

Figure: 1.5 Possible scheme of THF producing a side reaction[47]

As a result of all the findings listed above, biological and environmental studies aimed at investigating the impacts of *n*C_{60}, raised major concerns which began to accumulate within the scientific community on choosing the most relevant form of fullerene colloidal aggregates which have no possible side products or organic solvents which can contribute towards positive toxic impacts of C_{60}. Out of all synthesis methods, the AQU/*n*C_{60} method[10, 12] is the most relevant form of synthesis because of lack of organic decomposition products associated in other synthesis methods.

1.4 Inclusion complexes of C_{60} with cyclodextrin

Recently fullerenes have been of great interest in the scientific community to synthesize nanocomposites with linear, branched or networked polymers to enhance the matrix's mechanical,[50-53] electronic,[54] and photosensitization[55-59] properties. The first experimental report of an inclusion complex of C_{60} with a cyclodextrin (CD) dates back to 1992. Andersson[60, 61] showed that C_{60} was capable of forming a 1:2 complex with γ-CD in water. Embedding C_{60} in a suitable water soluble host molecule, such as cyclodextrin, first emerged in the literature as a solubilizing technique of achieving higher water solubility of the hydrophobic fullerenes. However, due to the presence of a hydrophobic inner cavity, CDs can either partially or entirely accommodate suitably-sized low molecular weight molecules or even polymers. Hydrophobic

and van der Waals interactions are the main driving forces behind the formation of these so-called host-guest inclusion complexes,[62] and cyclodextrins have frequently been applied in separation processes (e.g., for environmental protection), pharmacy, analytical sciences, and catalysis, as well as in the food, cosmetic, textile, and packaging industry. [62, 63]

Much of the research on the inclusion complexes of cyclodextrin and C_{60} has centered on γ-cyclodextrin due to the size compatibility with hydrophobic guest: C_{60} with atom-to-atom diameter of 0.7 nm (van der Waals diameter 1.0 nm) and the hydrophobic inner cavity of host; γ-cyclodextrin with 0.75-0.83 nm wide inner cavity. Cyclodextrins are a family of cyclic oligosaccharides composed of α-(1,4) linked glucopyranose sub units and α-, β-, and γ- CDs being the most widely used, containing six, seven and eight glucopyranose subunits, respectively, as shown in Figure 1.6.[62]

In recent years, CDs have been used as building blocks for the development of a wide variety of polymeric networks and assemblies for various applications such as targeted drug delivery, tissue engineering and medical diagnostics. Syntheses of covalently linked networks by combining polymers and cyclodextrins are well-known for their ability to tailor mechanical properties.[64-66]

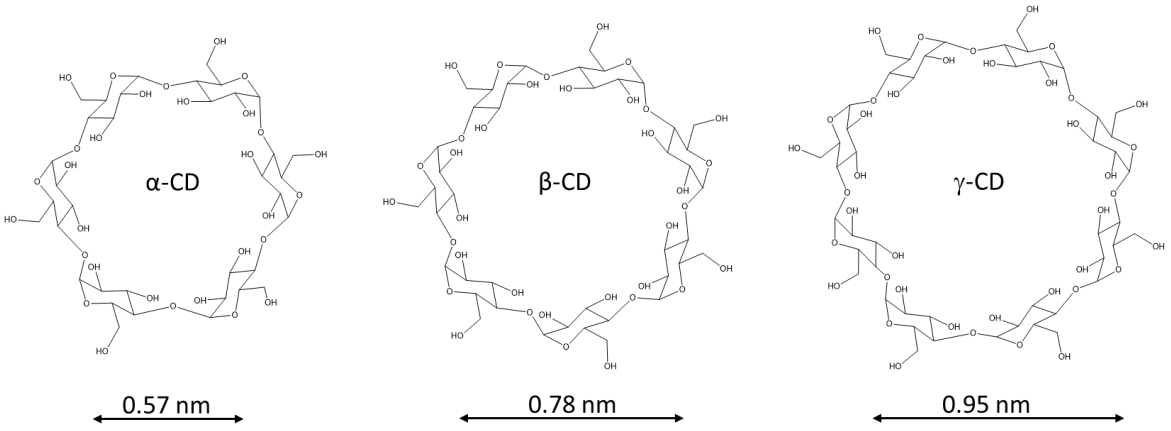

Figure 1.6 Chemical structures of α-CD, β-CD, and γ-CD

A recent study by Gaumani *et al.*[67] reported a synthesis route for alkyl-chain-modified α- and β-CDs by utilizing bifunctional reagents to achieve CD-based polymer networks. In a follow up study, the same group has synthesized cross-linked polymer networks by stable non-covalently bound polymeric inclusion complexes made from polypropylene oxide in β-cyclodextrin, followed by chemical crosslinking of the individual cyclodextrin moieties with bifunctional hexamethylene chains.[68] Furthermore, they have suggested that polymer networks formed in this manner might show excellent sequestration properties due to the high degree of freedom resulting from non-covalently bonded network nodal points.

The sequestration capability of a host, such as a cyclodextrin-derivatized network polymer matrix, will depend upon many desirable properties such as swellability, cross-link density, cross-link length of polymer chains, and possible guest-molecule interaction sites or pockets present in the network. One should also consider the solubility constrains among the host and the desired guest, such as C_{60} in this case, which play a major role in encapsulation versus preference to remain in the solution phase. It is therefore challenging to design such C_{60}-polymer nanocomposite networks with excellent guest-host capabilities.

1.5 Conclusions

In the literature there has been much debate about oxidative damage caused by *n*C_{60} suspensions. However, no study to date, has successfully evaluated the oxidation caused by AQU/*n*C_{60} suspensions in cell free conditions which measuring the rate of oxidation as a function of *n*C_{60} concentration, *n*C_{60} colloidal particle size, *n*C_{60} surface area, and $C_{60}O$ content, operating where necessary under inert and oxygen rich conditions. Also there are no reported data on

oxidation caused by *n*C_{60} samples that have been deliberately enriched with $C_{60}O$ compared to regular samples. Therefore it is clear that determining which attributes of fullerene suspensions drive the observed oxidative responses, as well as identifying the mechanisms underlying any observed oxidation, is of vital importance.

Thermal dependence or the thermally-activated transitions of *n*C_{60} suspensions has not been fully explained in reported literature. The main thermal reaction of fullerene species reported in literature is fullerene epoxide, $C_{60}O$, and its ability to form $C_{120}O$ with C_{60}.[69, 70] The effect of temperature on these colloids plays a significant role in both the synthesis and reactivity, and it is related to aggregation state that may be a vital factor in determining bioavailability.[25]

Motivated by the stringent requirements for making accurate kinetics and measurements on oxidation caused by AQU/*n*C_{60} colloidal dispersions, we have developed experimental methods utilizing dihydrorhodamine 123 (DHR123) as a sacrificial probe molecule to monitor oxidation by fluorescence spectroscopy and kinetic models to explain the observed oxidation. These experimental considerations are explained in Chapter 2 of this dissertation. Chapter 3 includes the method development, oxidation measurements, related reaction rate calculations and kinetic models that describe the *n*C_{60}'s oxidative behavior.

Investigations of thermal stability of *n*C_{60} colloidal dispersions prepared through all four primary *n*C_{60} synthesis methods are presented and compared in Chapter 4.

Additionally, this work has focused on developing and improving methods for the concentration determination of *n*C_{60} using comparative studies using high performance liquid chromatography (HPLC) and UV-Vis spectroscopy and is presented on Chapter 5 of this dissertation.

Finally, in Chapter 6, a research project conducted in collaboration with Dr. Jeffery White's research group at the Department of Chemistry at Oklahoma State University is

described. This work has focused on the synthesis and characterization of network polymer nanocomposites composed of C_{60} and dodecyl/γ-cyclodextrin to understand the guest-host interactions and the encapsulation efficiency of fullerenes.

CHAPTER II

EXPERIMENTAL PROCEDURES

2.1 Preparation of nC_{60} colloidal suspensions

2.1.1 AQU/nC_{60}

The synthesis of AQU/nC$_{60}$ was carried out according to a method similar to Labille.[10] Approximately 100 mg of C_{60} (sublimed, MER Corp., Tucson, AZ, MR6HP 99.9%) was added to a 500-mL conical flask with 200 mL of 18 MΩ water (Millipore, Billerica, MA, Direct-Q3 UV system 18 MΩ.cm @ 25°C). The flask was sealed tightly with a rubber stopper and stirred for three weeks. The resulting muddy-colored suspension was filtered through a 0.45 μm mixed cellulose esters (MCE) sterile filter (Fisher Scientific, Denver, CO) to remove any undispersed material and characterized by Dynamic Light Scattering (DLS) analysis for particle size, high performance liquid chromatography (HPLC) for derivative analysis and UV-Vis spectroscopic analysis for concentration determination. This stock suspension was used to study the thermal stability of colloids.

Synthesis and characterization of AQU/nC$_{60}$ suspensions for the evaluation of oxidative behavior was carried out using the same method discussed above, except with different amounts of starting materials to prepare four stock suspensions. In separate round-bottomed flasks was added 0.05 g, 0.1 g, 0.2 g and 0.3 g of C_{60} to 200 mL of 18 MΩ water, sealed tightly with a rubber stopper and stirred for about eight weeks.

2.1.2 $C_{60}O$-enriched AQU/nC_{60}

The procedure for the synthesis of $C_{60}O$-enriched solid was similar to that reported by Chibante.[71] To prepare a stock solution of C_{60}/toluene, approximately 200 mg of C_{60} was dissolved in 150 ml of toluene (PHARMCO-AAPER HRGC/HPLC-trace grade) and stirred overnight. The stock solution was diluted to obtain three, 100-mL aliquots of 400 ppm C_{60}/toluene and added to three separate 250-mL round-bottomed flasks. O_3-enriched O_2 was generated by enriching a 0.2 L/min stream of O_2 with ozone using an ozonator (Ozone Serviceozonator, Yanco Industries Ltd.) and diluting the resulting stream 4:1 by N_2 gas to a total flow rate of 1.0 L/min. A fraction of this gas mixture was bubbled through the C_{60}/toluene solutions at a flow-rate of 0.2 L/min for 15, 30 and 60 seconds, respectively, at room temperature with vigorous stirring. The samples were then stirred overnight. An aliquot (1 mL) from each sample was filtered through a 0.02 μm Whatman® Anatop™ filter (Fisher Scientific, Suwanee, GA) for HPLC derivative analysis. Toluene was removed from each sample by rotary evaporation to dryness (using a Heidolph® HB control rotavap) with an applied pressure of 40 mbar and temperature of 45 °C. The resulting $C_{60}O$-enriched solids were air dried for several days before further use.

To prepare the $C_{60}O$-enriched AQU/*n*C_{60}, a similar method was used as reported by Labille[10] except using the $C_{60}O$-enriched solids as the starting material. From each of the three different samples, approximately 130 mg of $C_{60}O$-enriched solids were added to three separate 500-mL round-bottomed flasks with 150 mL of 18 MΩ water. The flasks were sealed tightly with a rubber stopper and stirred for 12 days. Resulting muddy color suspensions were filtered separately through a 0.45 μm MCE sterile filter to remove any undispersed material. They were characterized by DLS analysis for particle size, HPLC for derivative analysis and concentration

determination. These three suspensions were stored as stock suspensions of $C_{60}O$-enriched AQU/*n*C_{60} for the evaluation of oxidative behavior of *n*C_{60} colloids.

2.1.3 SON/nC_{60}

For the synthesis of SON/*n*C_{60} the method adopted was a modification of the that developed by Andrievsky.[9] Approximately 100 mg of C_{60} was dissolved in 100 ml of toluene, and the solution was stirred overnight to obtain a 1 mg/mL solution of C_{60}/toluene. A 15 mL aliquot of C_{60}/toluene solution was transferred to a 155 mm long test tube with inner and outer diameter of 30 mm and 32 mm, respectively. Then sixty mL of 18 MΩ water was added to the test tube which was suspended in a sonication bath (Fisher Scientific FS140H, 185 W) and maintained at below 40 °C. The mixture was sonicated until all of the toluene evaporated and the color of the mixture changed from purple to brownish yellow. Multiple identical fractions were collected and combined and then were again sonicated for 2.5 hrs to ensure the removal of any traces of toluene. The resulting suspension was then filtered through a 0.45 µm MCE sterile filter to remove any undispersed material. The C_{60} suspension produced by this method was characterized by DLS analysis for particle size, HPLC analysis for derivative identification, and UV-Vis spectroscopic analysis for the determination of concentration.

2.1.4 THF/nC$_{60}$

For the synthesis of THF/*n*C$_{60}$, the method adopted was a modification of the method developed by Brant.[12] Approximately 25 mg of C$_{60}$ was dissolved in 100 ml of tetrahydrofuran (PHARMCO-AAPER HRGC/HPLC-trace grade, stabilized with BHT) and the suspension was stirred overnight. The resulting solution was filtered through a Whatman® glass microfiber filter (934-AH, 42.5 mm Ø, 1.5 µm pore size) to remove any undissolved material. The filtered solution was then added to a 500-mL round-bottomed flask, and 100 mL of 18 MΩ water was added to the rapidly stirred solution at a rate of 1 L/min. Upon the addition of water, the solution immediately changed color from light magenta to yellow, and the stirring was continued overnight. Approximately 100 mL of tetrahydrofuran was removed by rotary evaporation (using a Heidolph® HB control rotavap) with an applied pressure of 150-200 mbar and a temperature of 35 °C over approximately 20 min. To ensure the removal of all tetrahydrofuran, 25 mL of 18 MΩ water was added to the reaction flask, followed by the removal of an additional 20-25 mL of water achieved by reducing the pressure to 45 mbar at 40 °C. This process was repeated twice. The final suspension was filtered through a 0.45 µm MCE sterile filter to remove any undispersed material. The C$_{60}$ suspension produced was characterized by DLS analysis for particle size, HPLC for derivative analysis and UV-Vis spectroscopic analysis for the determination of concentration.

2.1.5 TTA/nC$_{60}$

The procedure for the synthesis of TTA/*n*C$_{60}$[12] was adopted almost exactly from Scrivens,[13] except for the replacement of benzene with toluene and ozonation of the starting

solution to achieve higher concentrations of *n*C_{60}. Approximately 10 mg C_{60} was dissolved in 100 ml of toluene, and the solution was stirred overnight. The O_3-enriched O_2 was generated by the ozonator (Ozone Serviceozonator, Yanco Industries Ltd.) in a 0.2 L/min stream of O_2, and the stream was diluted 4:1 by N_2 gas and a total flow rate of 1.0 L/min. A fraction of this gas mixture was bubbled through the above solution at a flow-rate of 0.2 L/min for 5 seconds at room temperature. This mixture was stirred overnight. Then ten mL of tetrahydrofuran was added to the resulting mixture which was stirred for 30 min, followed by the addition of 100 mL of acetone (PHARMCO-AAPER HPLC/UV grade) with another 30 min of stirring. Finally, 200 mL of 18 MΩ water was added to the mixture which was stirred overnight. Approximately 110 mL of solvent (mostly acetone) was removed by rotary evaporation with an applied pressure of 85 mbar and a temperature of 22 °C for approximately 30 minutes. Then twenty five mL of 18 MΩ water was added to the reaction flask, followed by the removal of an additional 20-25 mL of solvent achieved at a pressure of 85 mbar at 26 °C. This process was repeated twice. The resulting suspension was then filtered through a 0.45 µm MCE sterile filter to remove any undispersed material. Finally another rotary evaporation step was carried out to concentrate the collected *n*C_{60} suspension at 60 mbar and 50-53 °C for about 30 minutes. The C_{60} suspension produced was characterized by DLS analysis for particle size, HPLC for derivative analysis and UV-Vis spectroscopic analysis for determination of concentration.

2.2 Characterization Techniques

2.2.1 Particle size analysis

The size distribution of the fullerene colloidal particles was determined using DLS performed on a DAWN® HELEOS™ 243-HHC (Wyatt Technology Corp.) equipped with Ga-As laser (60 mW) operating at a wavelength of 658.0 nm at 25 °C. The measurements were performed at a 99° scattering angle at Detector #12. The samples used in the analysis were dilute and were contained in a 20 mL scintillation vials. The hydrodynamic radii of the colloidal particles were determined by a proprietary, non-negative least squares algorithm known as "regularization analysis" of the scattered light intensity autocorrelation function. This algorithm makes no prior assumptions about the shape or form of the size distribution.

For some colloidal samples, a Malvern High Performance Particle Sizer, model HPP5001 was used to determine the size distribution. For all the measurements using this instrument the dispersant was water which has a refractive index of 1.330 and viscosity of 0.8872 cP. All the measurements were done at 25 °C and using either a DTS0112 low volume disposable sizing cuvette or a DTS0012 disposable sizing cuvette.

2.2.2 C_{60} derivative analysis

Analysis of samples for C_{60} content and that of its derivatives was done using a HPLC system from Varian consisting of a 210 ProStar Solvent Delivery Module, a Rheodyne® 7725i injection valve with an injection volume of 20 µL and a 355 ProStar Photo Diode Array detector

with a deuterium (UV) and quartz iodide (visible) lamp source, all operating through a Galaxie™ Chromatography Workstation.

Extraction of C_{60} and its derivatives from the aqueous suspensions for HPLC analysis was performed by adding 2 mL of 10% (W/V) $NaNO_3$ and 1.5 mL toluene to 2-6 mL of *n*C_{60} (the amount will vary depending on the concentration of *n*C_{60}). The mixture was stirred overnight, and then the toluene and water layers were allowed to separate. The toluene layer was extracted and then dried using anhydrous Na_2SO_4, and filtered through a 0.02 μm Whatman® Anatop™ filter (Fisher Scientific, Suwanee, GA) before analysis on the HPLC. Samples showing absorption spectra from 300 nm to 450 nm were collected at all retention times. All HPLC chromatograms presented in this study were extracted at 336 nm, where the C_{60} spectrum had an intensity maximum. The analytical column used was a NacalaiTesque "CosmosilBuckyprep", Waters type, 4.6 x 250 mm packed column, protected by an equivalent 10 mm guard column. HPLC Grade toluene was used as the mobile phase with a flow rate of 1 mL/min.

To verify that all the C_{60} and its derivatives were extracted into toluene, the aqueous layer resulting from each extraction was analyzed by UV-Vis spectrophotometer Varian Cary 5000 (or Cary 100) at λ = 200-800 nm compared to a background of 1 mL of 18 MΩ water mixed with 2 mL of 10% $NaNO_3$.

2.2.3 Concentration determination of nC_{60} suspensions

Concentration determinations were primarily carried out using UV-Vis spectroscopy, and the calculations were based upon spectral matching with a standard spectrum of C_{60} dissolved in toluene. A HPLC concentration determination procedure has been used, with a calibration curve

of C_{60}/toluene standards which gave more accurate results compared to UV-Vis spectroscopic data, especially in cases where standard spectral matching was not satisfactory (see Chapter V for details).

In our UV-Vis spectroscopic procedure modified from Deguchi *et al.*,[15] 1 mL of the *n*C_{60} suspension, 2 mL of 10% (w/v) $NaNO_3$ and 3 mL of toluene were added to a 20-mL scintillation vial and sealed with a Teflon lined cap. The vial was suspended in a sonication bath for 10 min. The resulting mixture was set aside for 2-3 hours or overnight as needed to allow the layers to separate completely. The aqueous and the organic layers were then separated and analyzed by UV-Vis spectroscopy (Varian Cary 5000 UV/vis/NIR or Varian Cary 100 UV/vis). Samples were scanned from λ= 200-800 nm, using 18 MΩ water, 1 mL 18 MΩ water mixed with 2 mL of 10% (w/v) $NaNO_3$ or toluene as background samples as appropriate. Standard rectangular, 10 mm Quartz cuvettes (Starna cells, catalog # 1-Q-10) were used for the analysis. Complete extraction of fullerene into the toluene layer was verified by the absence of any measurable absorbance at wavelengths characteristic for C_{60} (e.g., λ = 336 nm) in aqueous layer. Concentration of C_{60} in the toluene layer was calculated by fitting the experimental absorbance curve to a calibrated reference spectrum of C_{60} in toluene according to Beer's law.

In the HPLC procedure (discussed in Chapter V under method development), six different C_{60}/toluene standard solutions were prepared (from gravimetric calculations) and analyzed for HPLC to determine the peak areas of the C_{60} peak for each concentration. A calibration curve was obtained for the peak area versus concentration of C_{60} standard, and this curve was used for the determination of unknown concentrations of C_{60} solutions.

2.3 Evaluation of Oxidative Behavior

2.3.1 Preparation of Dihydrorhodamine123 (DHR123) solution

Dihydrorodamine 123 (1.25 mg, Invtrogen™, Carlsbad, CA) was dissolved in 31.25 mL of ethyl alcohol (AAPER, ethyl alcohol USP, absolute 200 proof) to achieve a 40 ppm solution. To minimize the conversion of DHR123 to Rhodamine 123, the solution was sealed under nitrogen gas and stored in the dark at low temperature if not used. Prior to use, the DHR123 solution was thawed at ambient temperature in the dark.

2.3.2 Preparation of standard buffer solutions of pH = 4.6, 7.4 and 9

Each buffer capsule (pHydrion buffers, Micro Essential Laboratory, Brooklyn NY) of standard pH = 4.6, 7.4 and 9 (±0.05) was dissolved separately in 100 mL of 18 MΩ water, and the pH was measured using a pH meter to verify the final pH of the solution.

2.3.3 Preparation of $KMnO_4$ solution

Potassium permanganate (KMnO4, 0.115 mM, Fisher Scientific ≥99%) solution was prepared by dissolving 9.1 mg solid $KMnO_4$ in 500 mL of 18 MΩ water in a 500- mL volumetric flask. To facilitate the dissolution process, the flask was heated to about 60 °C, and the final

solution was filtered through a Whatman® filter. Solutions were stored in brown glass bottles in the dark and used within 1-2 days. For each new experiment fresh solutions were prepared as needed.

2.3.4 Evaluation of oxidation caused by nC_{60}

The oxidation behavior of nC$_{60}$ colloids was studied using fluorescence spectroscopy. The fluorescence intensity of rhodamine123 produced by the oxidation reaction was measured using a Fluorolog®-3 spectrofluorometer (HORIBA Scientific). Thus, 3 mL of pH = 4.6 buffer, 5 µL of DHR 123 and a micro stir bar were added in to a quartz fluorometer cuvette (Starna Spectrosil® Quartz 23-Q-10), and mixed thoroughly and finally, placed in the sample holder. Data was collected for 300 s with 0.1 s intervals and a 0.1 s integration time while the mixture was continuously stirred. At 300 s, a 500-µL aliquot of the nC$_{60}$ suspension was added to the mixture, while running the instrument, and mixed thoroughly by hand and placed in the fluorometer sample holder. Data acquisition was continued for another 1500 s with continuous stirring. Control experiments were carried out using the same procedure, except adding 18 MΩ water instead of our nC$_{60}$ sample. The wavelengths used for the excitation and emission of the sample were 485 nm and 530 nm, respectively. The exit and entrance slit widths on the instrument settings were adjusted to 3 nm. Experiments were performed in ambient, inert (under nitrogen) and oxygen conditions. For all experiments which were carried out under nitrogen or oxygen conditions, a screw cap cuvette equipped with a septum seal was used, and the samples were purged with nitrogen or oxygen gas for 15 min, as appropriate, and sealed. Some experiments were carried out in the presence and absence of a neutral density filter to attenuate the spectrofluorometer's excitation light. Different concentrations of colloidal nC$_{60}$ were used for the

experiment, and the suspensions were concentrated using rotary evaporation or Millipore Amicon Ultra Centrifugal Filter Units as needed.

In the method development stage, the oxidation of DHR 123 by $KMnO_4$ was studied using a similar procedure discussed above except using $KMnO_4$ in place of the nC_{60} sample. Oxidation caused by $KMnO_4$ was studied under all 3 different pH buffer conditions 4.6, 7.4 and 9.

2.4 Investigation of thermal stability of the nC_{60} colloidal suspensions

For this study, the colloidal suspensions prepared by Aqua/nC_{60}, SON/nC_{60}, THF/nC_{60} and TTA/nC_{60} methods were used to compare the effect of each method regarding the stability of these colloidal particles. The initial C_{60} concentration of each suspension was 5 ppm. Then fifty mL of sample was added to a 3-neck, round-bottomed flask with a magnetic stir bar. One neck of the flask was connected to a reflux condenser, the second neck was connected to a thermometer and the remaining one was kept sealed and attached to a 10-mL syringe for sampling the suspension, as shown in Figure 2.1. The round-bottomed flask was immersed in a water bath which was assembled on a hot plate with magnetic stirring, and a second thermometer was attached to measure the temperature of the water bath. Constant heating of the system was started at room temperature (~20 °C) with a ramp of 1 °C/min until any visual sedimenting or precipitation of the sample occurred or if not until water bath's temperature reached to the boiling point or close to 100 °C. After every 10 °C increase of temperature, a 4-mL volume was sampled from the suspension to analyze through dynamic light scattering. If there was no sedimenting or

precipitation observed, the water bath was kept at the boiling temperature for an hour to verify that there was no change occurred in the suspension.

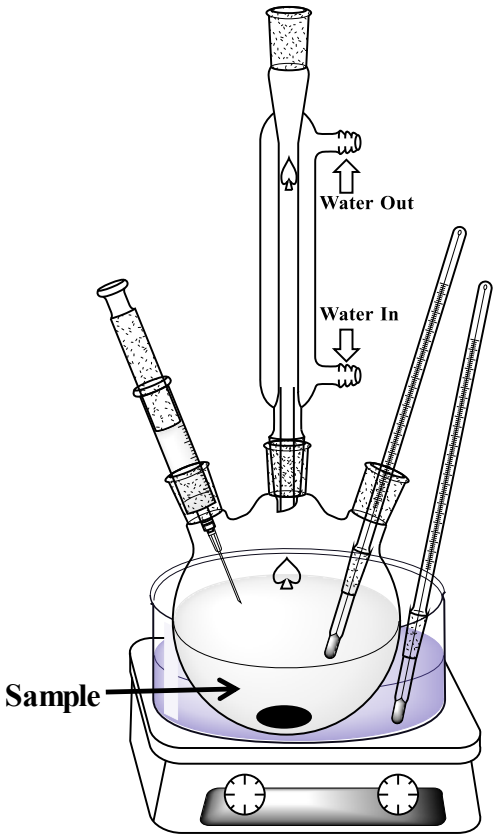

Figure 2.1 Experimental setup for the investigation of thermal stability

Additional experiments were carried out using $C_{60}O$ enriched AQU/*n*C_{60} to evaluate the thermal stability and the formation of $C_{120}O$ using HPLC. An aliquot of an AQU/*n*C_{60} sample was rotary evaporated until the suspension sedimented and/or went to dryness at 60 mbar pressure at 65 °C. Solid residue was dissolved in toluene and analyzed by HPLC for any detectable C_{60} dimers or polymeric species.

2.5 Fullerene Colloid Concentration Determination: Method Development

2.5.1 Preparation of C_{60}/toluene HPLC calibration series

A stock solution of 50 ppm C_{60} in toluene was prepared gravimetrically. For these gravimetric stock solutions, sublimed C_{60} was always used as the starting material to avoid problems caused by using standard as-received C_{60} material. Standard as-received C_{60} was purified by HPLC, and the purity quoted as 99.9% was not absolute, but relative to other fullerenes that was visible on HPLC. This was important because C_{60} forms clathrates with organic solvents,[72] often up to 5 toluene molecules per C_{60}. Hence to make gravimetric determinations reasonable, the use of sublimed C_{60}, which was free of clathrate-forming solvent molecules, was important.

A C_{60}/toluene standard series of 1, 2.5, 5, 10 and 20 ppm were prepared using the stock solution. All the standards were analyzed using HPLC. The chromatographic peak for C_{60} resulting from each standard was integrated using Galaxie™ software to achieve the peak areas in units of mAU·min. A calibration curve was developed using the concentration and the peak area data.

To test if there was an effect of small clusters of water being in the toluene layer that might cause differences in concentration while extracting it from aqueous colloidal suspensions into toluene, a second calibration curve was prepared using C_{60}/toluene standard series of 1, 5, and 20 ppm concentrations. Then two mL of each standard solution was sonicated with 2 mL of 18 MΩ water for 10 minutes and set aside for 2-3 h, or as needed, to allow the layers to separate completely. The toluene layers were dried using anhydrous Na_2SO_4 and filtered through a 0.02 μm Whatman® Anatop™ filter before analyzing on the HPLC.

2.5.2 Sample preparation for UV/Vis and HPLC comparisons

To evaluate the HPLC calibration curve method over UV/Vis spectroscopic procedure for concentration determination, four batches of samples were prepared by using a 5 ppm C_{60}/toluene stock solution. These experiments were designed in order to test the effects of mixing versus sonication, drying versus not drying and also the effect of adding $NaNO_3$ during extractions.

Two batches were prepared from 3 mL of the stock solution combined with 3 mL of 18 MΩ water in scintillation vials. One was sonicated using a sonicator bath for 10 min while the other was stirred for 10 min. The other two batches were prepared by mixing 3 mL of the stock solution, 2 mL of 18 MΩ water and 1 mL of 10% $NaNO_3$ in scintillation vials and treated with the same sonication and stirring procedures discussed above. All the vials were set aside for 2-3 h, or as needed, to allow the layers to separate completely. The toluene layers were dried using anhydrous Na_2SO_4 and filtered through a 0.02 μm Whatman® Anatop™ filter before analyzing using HPLC. In the UV/Vis spectroscopic analysis, the sample was divided into two aliquots where one was dried (anhydrous Na_2SO_4) before analyzing through UV/Vis spectroscopy.

2.5.3 Calculation of concentrations

For all HPLC data the C_{60} peaks were integrated, and the concentrations were determined using the HPLC calibration curve. For UV/Vis spectroscopic data, the experimental

absorbance curves were fitted to a calibrated reference spectrum of C_{60} in toluene according to Beer's law.

2.6 C_{60}-polymer nanocomposite networks

2.6.1 Synthesis of C_{60}/dodecyl/γ-cyclodextrin nanocomposite networks

In a typical synthesis, 20 mg (10.1 mmol) of the purified and dried dodecyl/γ-CD powder (provided by our collaborators Prof. Jeffery L. White and Dr. Gaumani Gyanwali) was placed in a 20-mL scintillation vial, and 5 mL of N,N-dimethylformamide (Sigma Aldrich, 99.8%), was added. The mixture was stirred overnight at room temperature until swelling of the dodecyl/γ-CD powder was observed to yield a cloudy suspension of swelled network polymer. In a separate vial, 2 mg (2.7 mmol) of C_{60} was stirred overnight in 5 mL of N,N-dimethylformamide (DMF) to yield a yellow-brownish solution. These reagent amounts corresponded to a C_{60}:γ-CD molar ratio of 1:3.6. Each vial was then stirred separately in a 60 °C water bath for 30 min, and the C_{60} mixture was added to the dodecyl/γ-CD network mixture and stirring was continued for another 3 h in the same water bath at 60 °C. The combined solutions were then stirred for an additional 15 h at room temperature. The resulted dark, brown/black solution was then filtered through a Whatman® filter using a vacuum filtration setup, and the filter paper was air-dried for overnight at room temperature. Following a wash with toluene to remove any free C_{60}, and subsequent drying, the film was removed from the filter paper using forceps. Henceforth, we refer to this as the "as-prepared" C_{60}/polymer composite network. Additional toluene washes were done to determine the stability of C_{60} in the network and were analyzed by UV-Vis spectroscopy to confirm the presence of C_{60} in the filtrates. To obtain the final film, washings with toluene were carried out until the characteristic peak for C_{60} disappeared from the UV-Vis spectrum.

Additional experiments were carried out starting with 1:1 and 2:1 C_{60}:γ-CD molar ratios to synthesize new films of this kind. Control experiments were carried out employing the same procedure without adding C_{60} to the mixture, and also a separate experiment replacing DMF with toluene in each dissolution, swelling and combination steps. Composite networks were also prepared using α-CD and C_{60} to investigate the uptake process of C_{60} by a network made-up with smaller cavities than γ-CD.

The ^{1}H-decoupled (75 kHz decoupling field strength) solid-state ^{13}C MAS (magic-angle spinning) NMR spectra of the dried network products were obtained using a Bruker DSX-300 spectrometer operating at 7.05 T field strength (300 MHz ^{1}H Larmor frequency). The ^{13}C, single-pulse (π/2 pulse width) data were obtained for all samples prepared, and, unless otherwise stated, 5 kHz MAS speeds were used. Cross-polarization (CP/MAS) spectra were acquired with 1 ms contact time and 75 kHz ^{1}H decoupling. Such spectra were collected by Dr. Gaumani Gyanwali.

2.6.2 UV/Vis spectroscopic analysis

The toluene solutions resulted from washing the film were analyzed by UV-Vis spectroscopy (Varian Cary 5000 UV/vis/NIR or Varian Cary 100 UV/vis). Samples were scanned from λ = 200-800 nm, using standard rectangular, 10 mm Quartz cuvettes. An empty cuvette was used to obtain the zero reading in the instrument, and pure toluene was used as the blank solution.

CHAPTER III

OXIDATIVE BEHAVIOUR OF *n*C_{60} COLLOIDAL SUSPENSIONS IN WATER

3.1 Introduction

As a result of continuing progress of nanotechnology, large quantities of fullerenes (C_{60}) are being produced, used, and potentially released into the environment.[73] For example C_{60} is currently being produced in multi-ton quantities by Frontier Carbon Corporation (FCC) in Japan, for fuel cell applications.[7] Previous studies have revealed that pristine (underivatized) fullerenes, derivatized fullerenes and colloidal suspensions of fullerenes are candidates for health and environmental hazards.[74, 75] Substantial data have been appeared in the literature leading to conflicting interpretations of this material's toxicity.[11, 16, 34, 35, 37-40, 43, 47, 76-80] The original studies on the cytotoxicity of fullerene colloids (*n*C_{60}) directly measured the results of oxidative damage and therefore found it to be an oxidant,[34-36] while others studies which reported anti-oxidant activity, or distinct lack of oxidation, were in fact measuring the reactive oxygen species (ROS) proxies.[37, 39] Some later reports attributed this oxidation entirely to contaminants present in fullerene colloidal suspensions, such as decomposition products of tetrahydrofuran as a result of the synthesis procedures utilized.[36, 38-41, 43-45] Therefore, ascertaining which attributes of fullerene suspensions drive the observed oxidative responses, as well as identifying the mechanisms underlying any observed oxidation, is of vital importance.

Due to the propensity of fullerenes to form stable colloidal suspensions in water prepared by starting from either organic solution of C_{60} or dried powder,[9-11] the two forms in which fullerenes are usually disposed of, colloidal suspensions of C_{60} were recognized to be the most environmentally and biologically relevant form of fullerenes. Consequently, the colloidal aggregates of this material become a critical starting point and a fundamental comparative model for fullerene-related studies. In particular colloids prepared by AQU/*n*C_{60} method (described in Chapter 2) are ideal candidates for the investigation of oxidative behavior because of the lack of organic decomposition products which act as oxidants. Furthermore, as reported by Murdianti[31] the presence of [6,6]-closed epoxide $C_{60}O$ in these AQU/*n*C_{60} colloids, in which the amount can be altered during preparation, can be used as another constraint to monitor oxidative responses resulting from these colloids.

The objective of this study is to evaluate the oxidative behavior and mechanism of fullerene colloids prepared by AQU/*n*C_{60} method by determining the oxidation rate as a function of *n*C_{60} concentration, *n*C_{60} surface area, number of colloid particles and $C_{60}O$ content, operating where necessary under an inert atmosphere and oxygen rich conditions. Furthermore, in this study colloid samples deliberately enriched in $C_{60}O$ have also been studied for oxidative behavior for comparison to regular AQU/*n*C_{60} suspensions. Detection of oxidative response has used dihydrorhodamine 123 (DHR123) as a sacrificial, non-fluorescent probe molecule which, upon oxidation, yields Rhodamine 123 (Rh123), a fluorescent cationic and lipophilic molecule ($\lambda_{excitaion}$ = 485 nm; $\lambda_{emission}$ = 530 nm) as described in Figure 3.1.

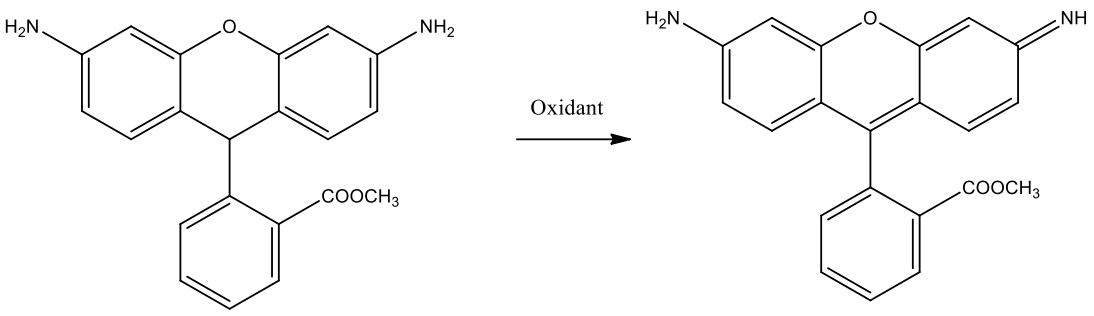

Figure 3.1 Conversion of dihydrorhodamine 123 into rhodamine 123 by an oxidant

3.2 Method Development

Development of a sensitive method to evaluate the oxidation caused by *n*C_{60} suspensions was modeled from using a similar approach that is used in biological studies. In the traditional view, oxidative damage in biological systems mainly occurs through reactive oxygen species (ROS) intermediates. Most commonly, ROS is detected by quantifying products of their reactions with probe-assisted spectroscopy, such as fluorescence, luminescence, spectrophotometry and electron spin resonance. Methods, such as measuring absorbance, are the simplest for detecting ROS. For example one classic way to detect and quantify superoxide production is via reduction of cytochrome *c* leading to increased light absorption at 550 nm.[81] However, due to higher sensitivity offered by fluorescence, a zero-background technique, fluorescent probes are more widely used in practice.[81] There are a variety of fluorogenic probes for assaying ROS mediated oxidative damage such as 2',7'-dichlorodihydrofluorescein diacetate (H_2DCFDA), derivatives of H_2DCFDA, aminophenyl fluorescein (APF), hydroxyphenyl fluorescein (HPF), dihydrorhodamine 123, dihydrorhodamine 6G, dihydrocalcein, dihydroethidium and 10-acetyl-3,7-dihydroxyphenoxanine (AmplexRed).[81-83] For this study dihydrorhodamine 123 was chosen from this menu of options for several reasons. It is sensitive to oxidative damage caused by both

ROS mediated routes and non-ROS mediated routes, is usable in aqueous media, and prior initial data recorded in our lab appeared promising. DHR 123 has been introduced in the late 1980s and first used by Rothe et al. in 1988 as an indicator of neutrophil respiratory burst,[84] and it has historically been used to evaluate oxidative damage.

During the development of the method, the first step was to understand the reactivity of the probe molecule towards an oxidant in terms of reaction time scale and reaction conditions. In order to get a better handle on the probe, we first evaluated its reaction with some common oxidants including $KMnO_4$, H_2O_2 and $FeCl_3$. Both H_2O_2 and $FeCl_3$ showed very slow reactions with DHR 123, which suggested they weren't suitable for short time scale kinetic studies. In contrast, $KMnO_4$ was a strong oxidant for DHR 123, and the reactions were completed within a 15-20 min time scale and plateaued as observed by fluorescence measurements. Figure 3.2 depicts a typical fluorescence kinetic trace of reaction with $KMnO_4$.

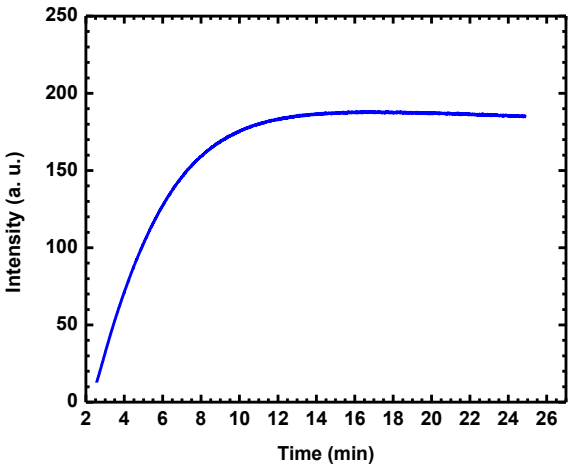

Figure 3.2 Fluorescence spectrum of reaction with 3.55 µM $KMnO_4$ with 0.178 µM DHR 123 recorded at an excitation and emission wavelengths of λ = 485 and 530 nm

Furthermore during method development we were able to optimize reaction conditions such as using a pH = 4.6 buffered medium and stirrer speeds sufficient to obtain smooth kinetic data.

3.3 Results and Discussion

3.3.1 Formation of AQU/nC_{60}

To evaluate the oxidative behavior of AQU/*n*C_{60}, five different colloidal suspensions were prepared and characterized using HPLC, UV/Vis spectroscopy and dynamic light scattering.

HPLC chromatograms of the toluene layers from each extraction revealed a primary peak at retention time of approximately 9 min and a small peak following that at a retention time of approximately 10 min as shown in Figure 3.3.

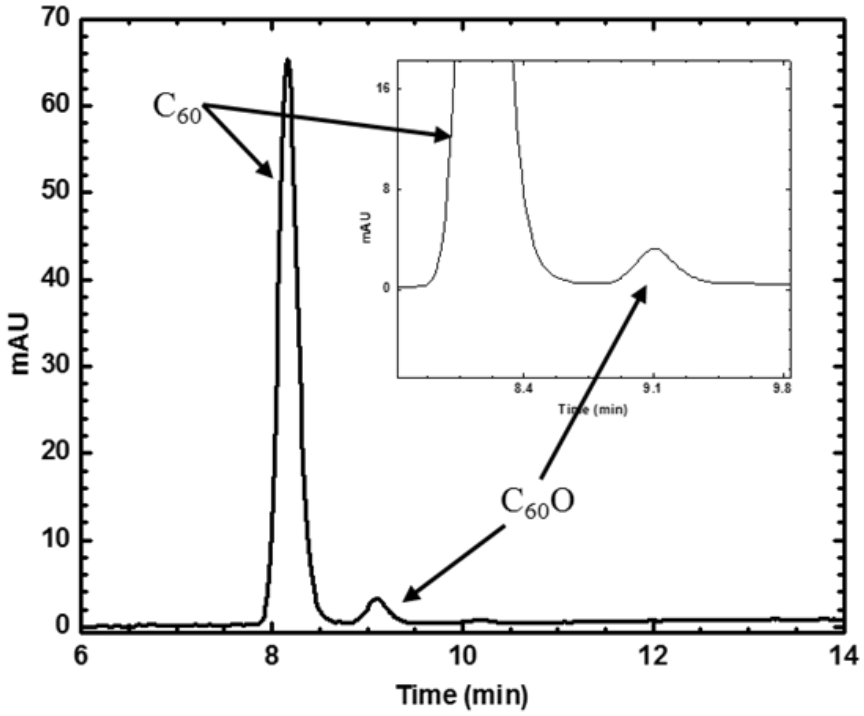

Figure 3.3 HPLC chromatogram at 336 nm from a toluene extraction of AQU/*n*C_{60} sample showing the elution of C_{60} and $C_{60}O$

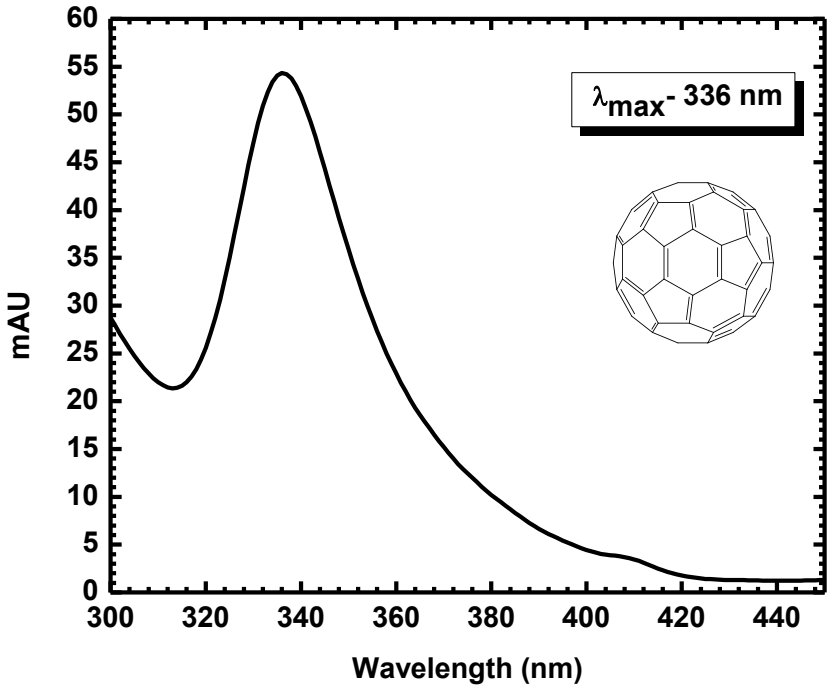

Figure 3.4 UV/Vis spectrum of C_{60} in toluene showing the absorbance maximum at 336 nm

As evident from Figure 3.4, peak eluted at 9 min has a visible absorption maximum at 336 nm, which matches the expected visible absorption maximum for C_{60} reported in literature.[11, 31] The peak that eluted at 10 min had a visible absorption maximum at 328 nm as shown in Figure 3.5, and which corresponded to the $C_{60}O$, the [6,6]-closed epoxide as reported in previous findings.[11, 31]

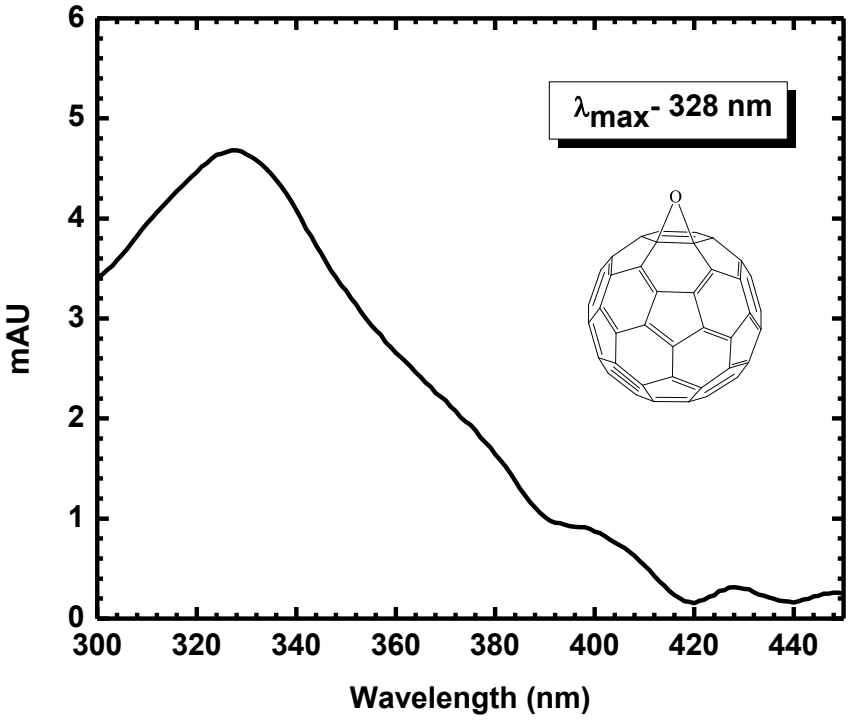

Figure 3.5 UV/Vis spectrum of $C_{60}O$ in toluene showing the absorbance maximum at 328 nm

The concentration calculated by the HPLC calibration curve method and the mean hydrodynamic radii (R_h mean) of particles for each suspension were shown in Table 3.1. Surface area and number of colloidal particles present in 1 L of suspension were calculated using the concentration of C_{60}, density of solid C_{60} and assuming colloids to be spherical in suspension. The amount of $C_{60}O$ present in each sample was calculated by multiplying the % area of the $C_{60}O$ peak given by HPLC by the corresponding C_{60} concentration.

$[C_{60}]$ (ppm)	R_h mean (nm)	Surface area per 1 L of suspension (cm^2)	number of particles per 1 L of suspension	% Area of $C_{60}Ox[C_{60}]$
0.595	63.17	164.32	$3.28x10^{11}$	1.85
1.19	63.17	328.64	$6.55x10^{11}$	3.71
3.25	67.16	844.25	$1.49x10^{12}$	5.79
3.78	76.95	857.70	$1.15x10^{12}$	7.69
4.80	73.79	1134.30	$1.66x10^{12}$	25.96

Table 3.1 Concentration, R_h mean, surface area, number of particles and % area of $C_{60}O$ x$[C_{60}]$ for five different suspensions of nC_{60}

Although we have characterized the suspensions using the parameters listed in Table 3.1, those parameters are interdependent. For example, changing the concentration of C_{60} will change the amount of $C_{60}O$ present in the sample and also the particle size, thus the surface area of colloids. Controlling these parameters independently is therefore difficult. Furthermore, most simple kinetic models assume free-floating and solution-phase reactants, where in our case we have colloidal aggregates. Thus, we may have to deal with the diffusion of particles rather than individual molecules, adsorptive sites on the particles, reactive sites on the particles, etc. Those are not parameters that we have easy access to.

3.3.2 Oxidative Behavior

Oxidative behavior of the AQU/nC_{60} suspensions was studied using triplicate measurements for each sample under fluorescence spectroscopy using the probe molecule DHR

123. Introduction of the oxidant, in this case the AQU/nC$_{60}$ suspension, increased the fluorescence intensity of the molecular probe as observed by the fluorometer. A typical fluorescence kinetic trace containing raw data obtained for an oxidation observed for added AQU/nC$_{60}$ and a control experiment done using 18 MΩ water instead of oxidant are shown in Figure 3.6a and 3.6b, respectively.

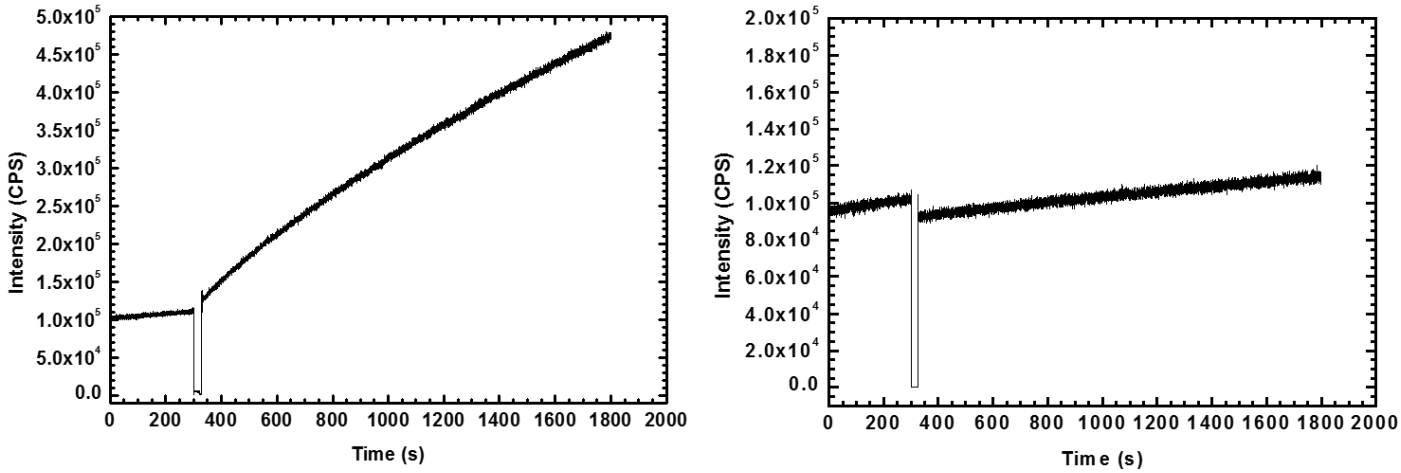

Figure 3.6 Fluorescence kinetic trace showing raw data (a) with added oxidant AQU/nC$_{60}$ and (b) with 18 MΩ water from the oxidation study

By comparing the two cases with and without an added oxidant, noticeable increase in fluorescence was observed in the case of added AQU/nC$_{60}$, which confirmed the oxidative ability of these suspensions. As shown in Figure 3.6a and 3.6b there was an initial loss of fluorescent data for a short period of time (about 20-30 s) due to removal of the sample cuvette in order to add the oxidant or 18 MΩ water and shake it thoroughly by hand to verify adequate mixing to achieve smoother data. Before conducting this mixing procedure, the data collected from the

kinetic study was extremely wavy which caused major problems in kinetic data analysis as shown in Figure 3.7.

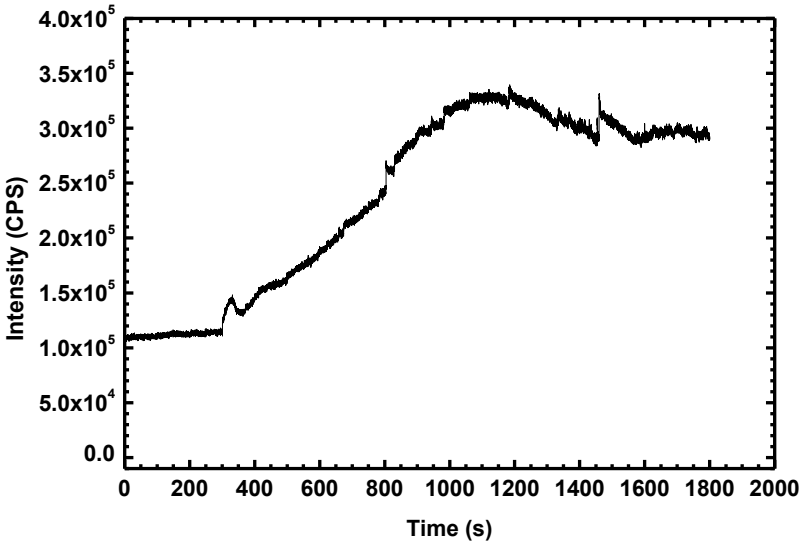

Figure 3.7 Fluorescence kinetic trace showing wavy data

Consequently, even at the expense of early time data, this special mixing procedure has been followed in all data collection steps. Moreover, as seen from Figure 3.6a, there is an initial measured fluorescence in the data even before the addition of AQU/*n*C_{60} due to the presence of rhodamine as a result of auto-oxidation of DHR 123. This is one of the disadvantages of using dihydro compounds as fluorescent probes.[85] To account for this background fluorescence and also the dilution occurring at the point of addition of the oxidant, the raw data was treated to obtain the accurate amount of oxidation (yellow colored area in schematic 1) contributed to the added oxidant as shown in Figure 3.8.

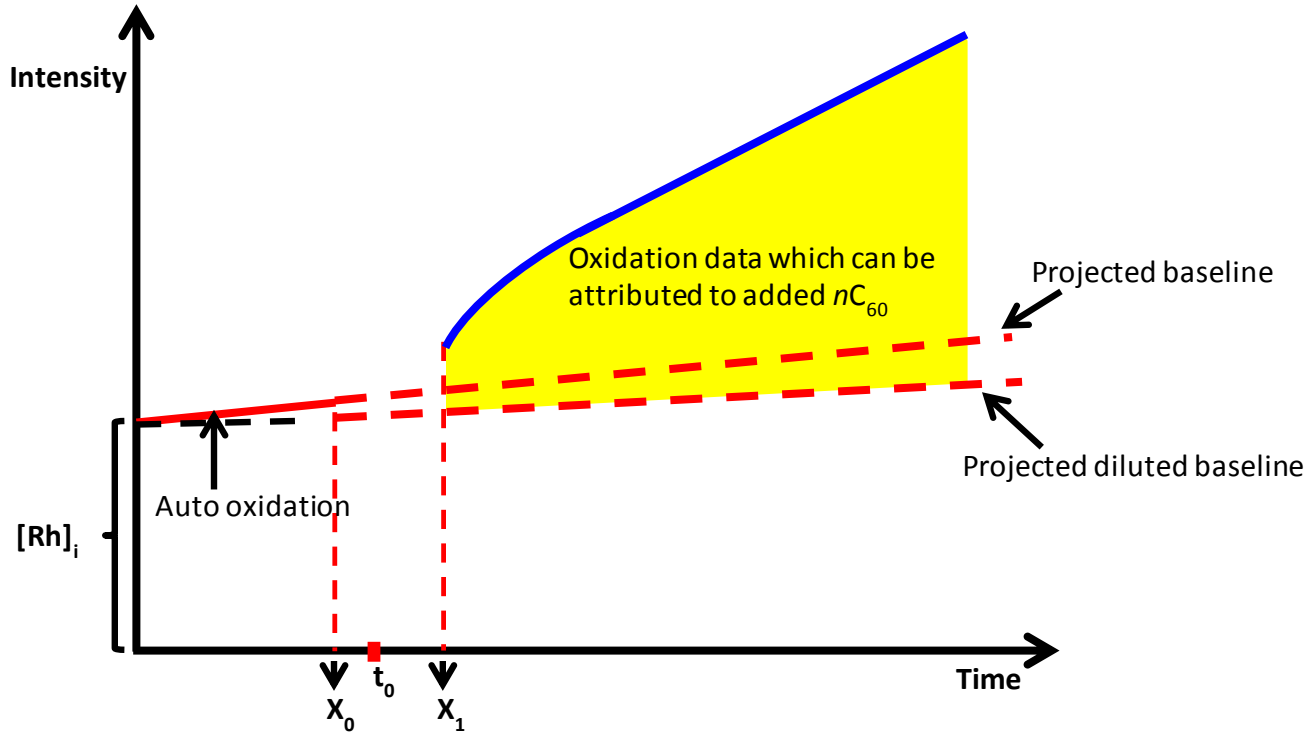

Figure 3.8 Schematic of treatment of raw data to obtain oxidation contributes to the added oxidant

With increasing the concentration of AQU/nC$_{60}$ an increase in measured, baseline corrected fluorescence intensity and slope was observed as shown in Figure 3.9. This observation concluded that there is definitely an oxidation occurring solely due to the added AQU/nC$_{60}$. Although the data were only acquired for a 30 min time scale which was adequate for the kinetic analysis, a typical oxidation run required 10-12 hours to complete as shown in Figure 3.10, which suggested that the reaction with AQU/nC$_{60}$ was slow compared to that with $KMnO_4$ which was expected to be a quite stronger oxidizing agent than AQU/nC$_{60}$.

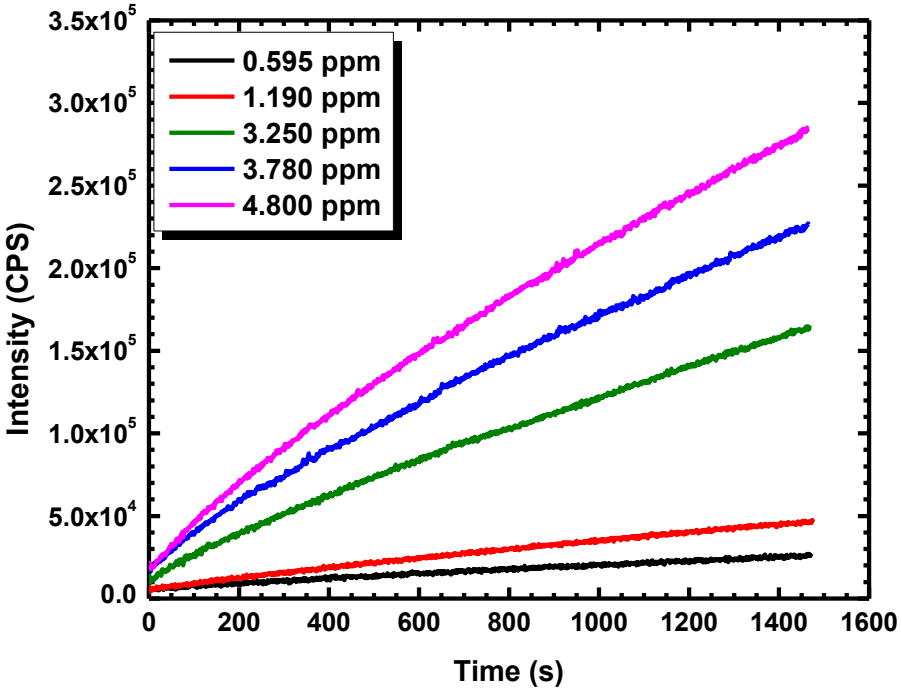

Figure 3.9 Fluorescence kinetic traces collected for different concentrations of AQU/*n*C_{60} reacted with an equal amount of DHR 123

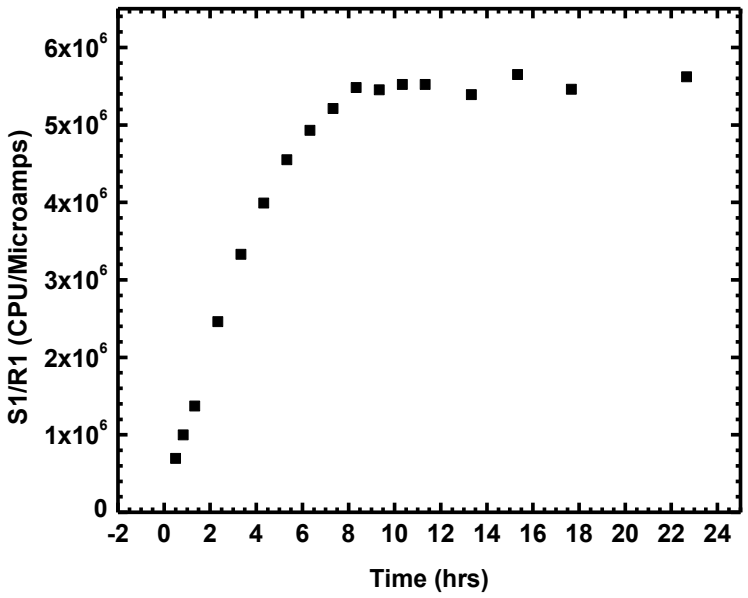

Figure 3.10 Fluorescence spectrum showing the completion of oxidation reaction between DHR 123 and AQU/*n*C_{60}

The most important feature observed from the raw data was that there was a rapid increase of fluorescence intensity just after addition of AQU/*n*C_{60} and a prominent initial curvature to the data with all the samples. This observation strongly suggested that there should be a fast component and a slow component for this observed oxidation reaction. Direct monitoring of the fast component was not achievable due the early-time data lost during the hand-mixing of the samples.

Due to the fact that the oxidation might be a sum of a fast and a slow component, the kinetic models, such as simple first order and simple second order, were not plausible for this system. Furthermore, the method of flooding[86] could not be used because controlling

concentrations of AQU/nC$_{60}$ system was difficult and the method of initial rates[86] could also not be used due to the loss of early time data. Therefore, to explain the observed kinetic behavior, the first model that was developed using sum of two exponentials, was shown by the equations below.[86] OriginPro 8 software was used to fit the data to this analytical model.

$$A \Rightarrow B$$

$$[A]_t = [A]_0 e^{-kt} \quad (1)$$

$$[A]_0 = [A]_t + [B]_t$$

$$[B]_t = [A]_0 - [A]_t \quad (2)$$

Both A and B are concentrations of DHR 123 and Rh 123, respectively. By substituting equation (1) in to equation (2), equation (3) was achieved as shown below.

$$[B]_t = [A]_0 - [A]_0 e^{-kt}$$

$$[B]_t = [A]_0 (1 - e^{-kt}) \quad (3)$$

$$y = [B]_{t_1} \left(1 - e^{-k_1 (t - t_0)}\right) + [B]_{t_2} \left(1 - e^{-k_2 (t - t_0)}\right) \quad (4)$$

Equation (4) describes the final form of the kinetic model that has been used to fit the baseline corrected data. Representative fitting curves resulted from this model are shown in Figure 3.11a, 3.11b and 3.11c.

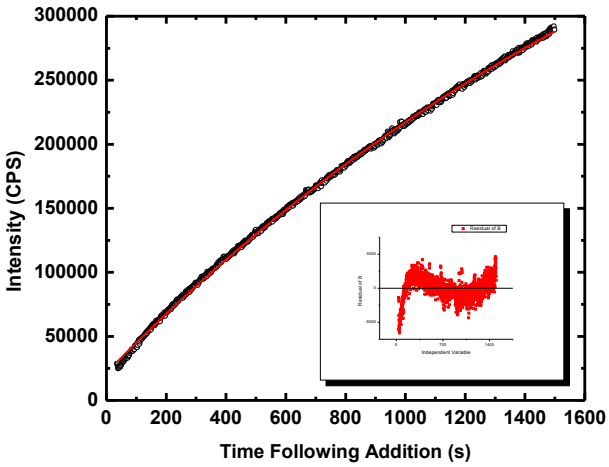

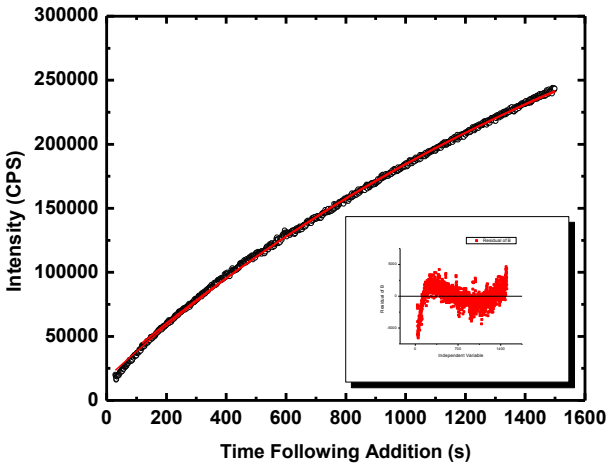

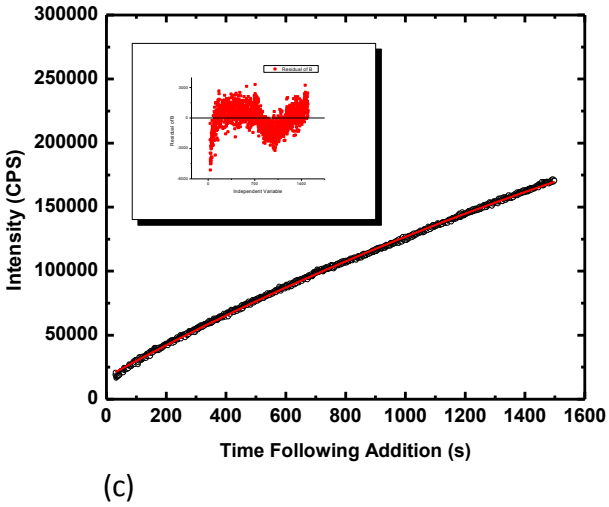

Figure 3.11 Experimental data fitted with the kinetic model, with the sum of two exponentials

To verify the precision of fitting curve versus actual data, residuals were plotted for each graph and are shown in the inset of each graph. Residuals are described as the difference between a particular data point to its fit at each data point plotted along the x-axis. This is helpful in identifying systematic errors in fits. As evident from Figure 3.11, the data points shown in

residuals were not evenly scattered around the x-axis, which clearly suggested that the fit contained systematic errors, and the model do not fit the data sufficiently.

The next analytically solvable model used to explain the data was a second order kinetic model using OriginPro 8 software as shown by the equations below.[86] While a single second-order component is unlikely to be successful, given the aforementioned fast and slow components, this model exhausts the simple, analytically-solvable kinetic schemes that can be easily tested by these methods.

$$A + B \Rightarrow C$$
$$R = -\frac{d[A]}{dt} = k[A][B]$$

These, A, B and C are concentrations of DHR 123, *n*C_{60} and Rh 123, respectively. To integrate the rate law for this model, it was convenient to define a progress variable *x* which measured the progress of the reaction to product as,

$$x = ([A]_0 - [A]_t) = ([B]_0 - [B]_t)$$

Both $[A]_0$ and $[B]_0$ were the initial concentrations. The rate expression given by equation can then be rewritten in terms of *x* as,

$$\frac{dx}{dt} = k([A]_0 - x)([B]_0 - x)$$
$$\int_{x(0)}^{x(t)} \frac{dx}{([A]_0 - x)([B]_0 - x)} = k\int_0^t dt$$

By solving the both sides of the integral the following solution can be obtained,

$$\frac{1}{([A]_0 - [B]_0)} \ln\left(\frac{[B]_0[A]_t}{[A]_0[B]_t}\right) = kt$$

$$[C]_t = [A]_0 - [A]_t$$
$$[A]_t + [C]_t = [A]_0$$
$$[B]_t = [B]_0 - [C]_t$$

By substituting $[A]_t$ and $[B]_t$ in terms of $[C]_t$ which was the rhodamine concentration at time, t, the following equation was obtained.

$$[C]_t = \frac{[A]_0[B]_0 e^{k([A]_0 - [B]_0)t} - [A]_0[B]_0}{[A]_0 e^{k([A]_0 - [B]_0)t} - [B]_0}$$

Representative fitting curves resulted from this second order model are shown in Figure 3.12a and 3.12b. It was evident from the main graph and the residuals that the data were not effectively fitted with the modeled parameters.

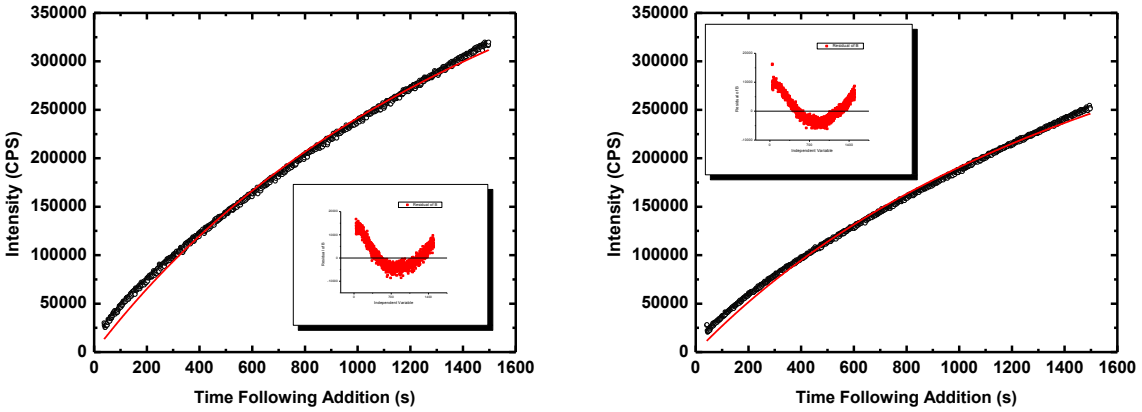

(a) (b)

Figure 3.12 Experimental data fitted with the second order kinetic model

Both kinetic models, the sum of two exponentials and the second order, were not sufficient to explain the oxidative behavior shown by these colloids. More sophisticated models are generally not analytically solvable, requiring numerical integration of the coupled differential rate equations. Therefore, the next model we selected was a pair of parallel second-order reactions, where C_{60} (or something whose concentration is proportional to C_{60}) and an unknown

component each independently cause the oxidation of DHR 123 to Rh 123. The resulting coupled differential rate equations were numerically integrated using Wolfram Mathematica 9.0.1 software. The model developed, using two parallel second order processes and their differential rate equations, are shown below, where A_2 represented the AQU/nC$_{60}$ and A_4 was an unknown species which was expected to have a relation to AQU/nC$_{60}$ and have concentrations proportional to the particular Aqua/nC$_{60}$ concentration.

$$DHR + A_2 \xrightarrow{k_1} Rh \tag{1}$$

$$DHR + A_4 \xrightarrow{k_2} Rh \tag{2}$$

$$\frac{d[DHR]}{dt} = -k_1[DHR][A_2] - k_2[DHR][A_4]$$
$$\frac{d[A_2]}{dt} = -k_1[DHR][A_2]$$
$$\frac{d[Rh]}{dt} = k_1[DHR][A_2] + k_2[DHR][A_4]$$
$$\frac{d[A_4]}{dt} = -k_2[DHR][A_4]$$

A representation of the fitting curves resulted from above model were shown in Figure 3.13a, 3.13b and 3.13c. The residual data shown for each fit was evenly distributed along the x-axis, compared to previous models, suggesting that the modeled parameters were sufficient to fit individual data sets obtained from oxidation.

To better evaluate this model, the rate constants were compared along multiple data sets, with the expectation to observe similar rate constants across multiple data sets. The rate constants obtained for the slow component of the oxidation reaction are shown in Table 3.2.

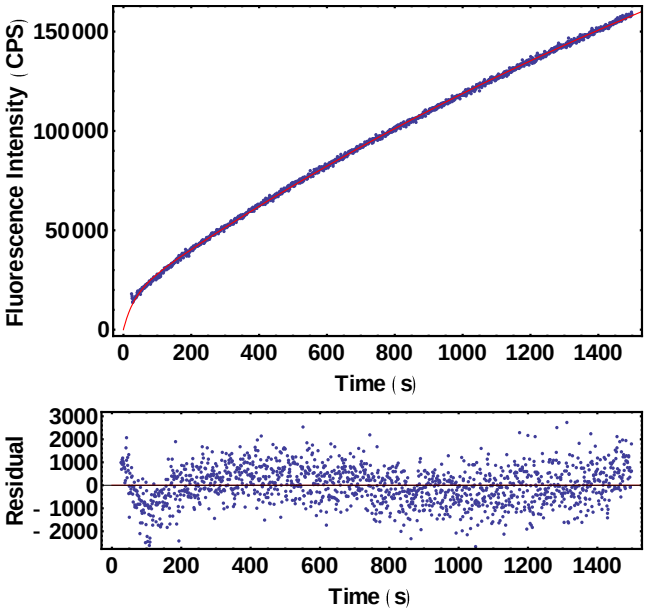

(a)

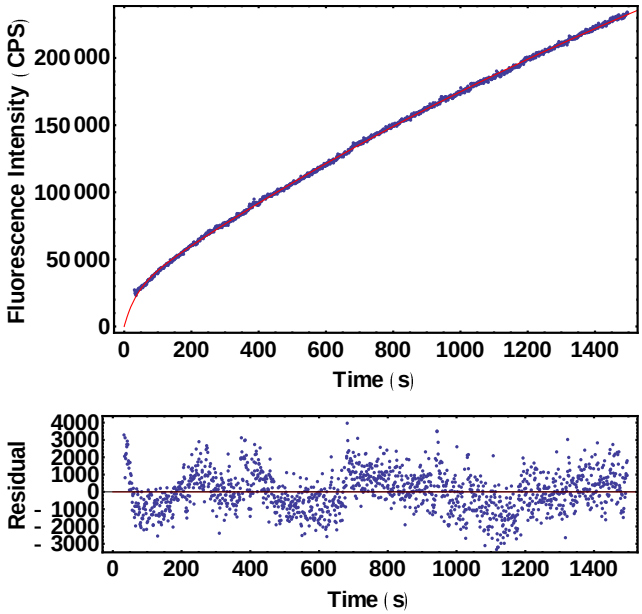

(b)

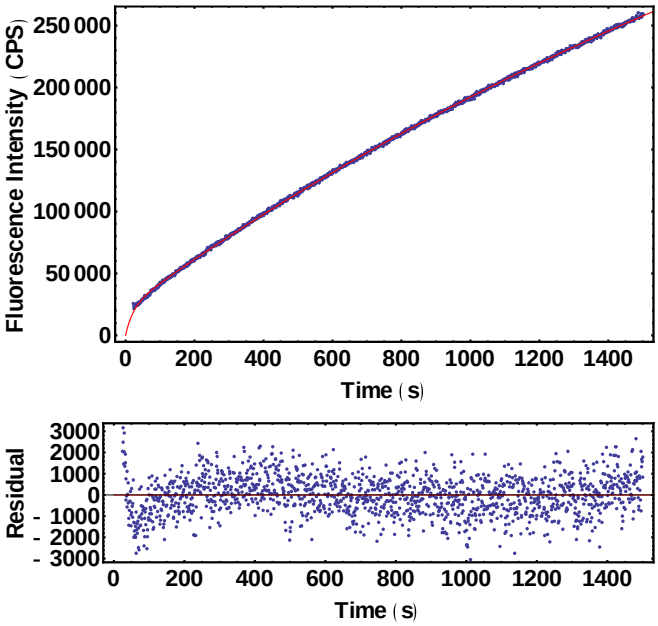

(c)

Figure 3.13 Experimental data fitted with the numerically integrated coupled differential rate equations method

$[C_{60}]$ (ppm)	k_1 ($M^{-1}s^{-1}$)	k_1 average ($M^{-1}s^{-1}$)	σ average
	198		
0.595	126	154	38.76
	137		
	257		
1.19	260	265	11.73
	279		
	352		
3.25	411	409	56.03
	464		
	390		
3.78	472	423	43.28
	407		
	324		
4.80	341	361	49.52
	417		

Table 3.2 Rate constants k_1 and σ for multiple data sets using two parallel second order differential rate equations

At different concentrations of AQU/*n*C_{60}, the rate constant k_1 calculated by the model was different. As seen from Figure 3.14, the rates were different outside of their statistical error, which suggested that the procedure developed was reproducible, but the kinetic model needed to be modified in order to draw conclusions on mechanistic understandings.

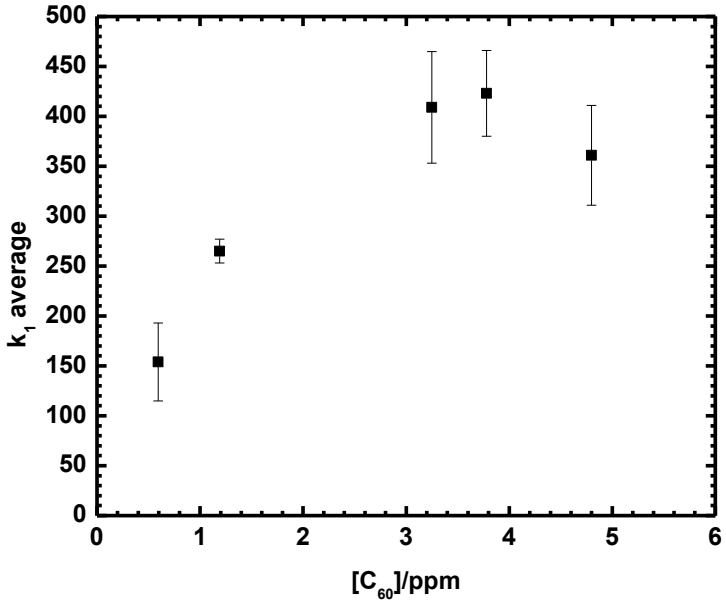

Figure 3.14 Graph of average k_1 vs concentration of C_{60} in different AQU/*n*C_{60} samples

When considering the fast component observed during oxidation, the scattering in k_2 across multiple data sets was even more apparent compared to k_1. Due to the fact that actual data for the fast reaction was not achievable during oxidation run, this observation was anticipated. The rate constants calculated for the fast component are shown in Table 3.3, and the graph showing the plotted $k_2 x[A]_4$ versus AQU/*n*C_{60} concentration is shown in Figure 3.15. Coefficient was the vertical scaling factor used in the fitting model.

$[C_{60}]$ (ppm)	k_2 ($x10^5$) ($M^{-1}s^{-1}$)	$[A_4]$ ($x10^{-9}$) (M)	$k_2x[A_4]$ ($*10^{-4}$) (s^{-1})	$k_2x[A_4]$ average ($x10^{-4}$) (s^{-1})	σ ($x10^{-4}$) average	Coefficient ($x10^{12}$)
	2.46	3.59	8.83			3.68
0.595	9.30	1.57	1.46	4.58	3.82	3.97
	1.42	2.42	3.44			2.51
	2.86	1.88	5.38			3.29
1.19	1.14	5.68	6.48	6.24	0.772	1.05
	1.14	6.02	6.87			0.984
	1.73	5.64	9.76			3.39
3.25	1.65	5.41	8.93	10.4	1.81	2.97
	1.88	6.59	12.4			2.56
	1.66	6.88	11.4			3.80
3.78	1.95	6.90	13.5	13.2	1.61	3.12
	2.73	5.35	14.6			4.15
	1.00	5.88	5.88			4.57
4.80	6.55	7.52	4.93	6.76	2.40	3.65
	1.41	6.72	9.48			4.49

Table 3.3 Rate constants k_2 for multiple data sets using two parallel second order differential rate equations

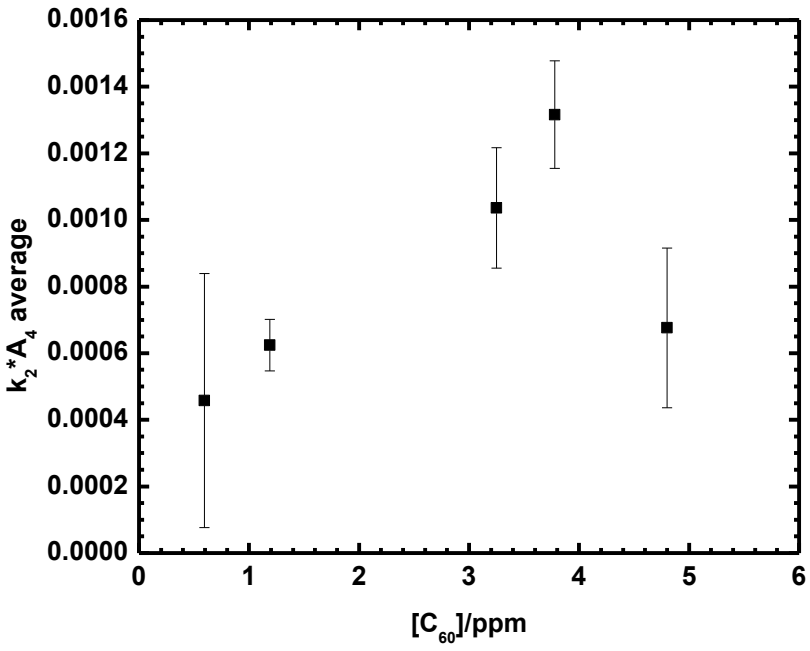

Figure 3.15 Graph of average $k_2x[A]_4$ vs concentration of C_{60} in different AQU/*n*C_{60} samples

3.3.3 Photo-induced oxidation and oxidation under modified atmosphere

To examine the possibility of photo-induced oxidation in the system discussed above, a separate set of experiments was conducted. A neutral density filter, a filter that reduces the intensity of all wavelengths of light equally, was used to reduce the excitation light which reached the sample. At the excitation wavelength of 485 nm, the light reaching to the sample was reduced to 39% in the presence of a neutral density filter. As expected, a reduction of the fluorescence signal intensity proportional to a change of approximately 39% was observed during oxidation. A

sample run in air under both conditions, with and without neutral density filter maintaining other parameters constant, is shown in Figure 3.16a. The data in the red curve was multiplied by 0.39 to see what the data would look like if we artificially attenuated it without changing the kinetics. The resulting curves do not overlap, indicating that there is a light-based contributing factor to the kinetics as shown in Figure 3.16b.

The effect of modified atmosphere on oxidation was studied under three different atmospheric conditions, namely pure nitrogen, pure oxygen, and normal atmosphere. Rate constants calculated for these reactions, combined with the presence and absence of neutral density filter, are summarized in Table 3.4.

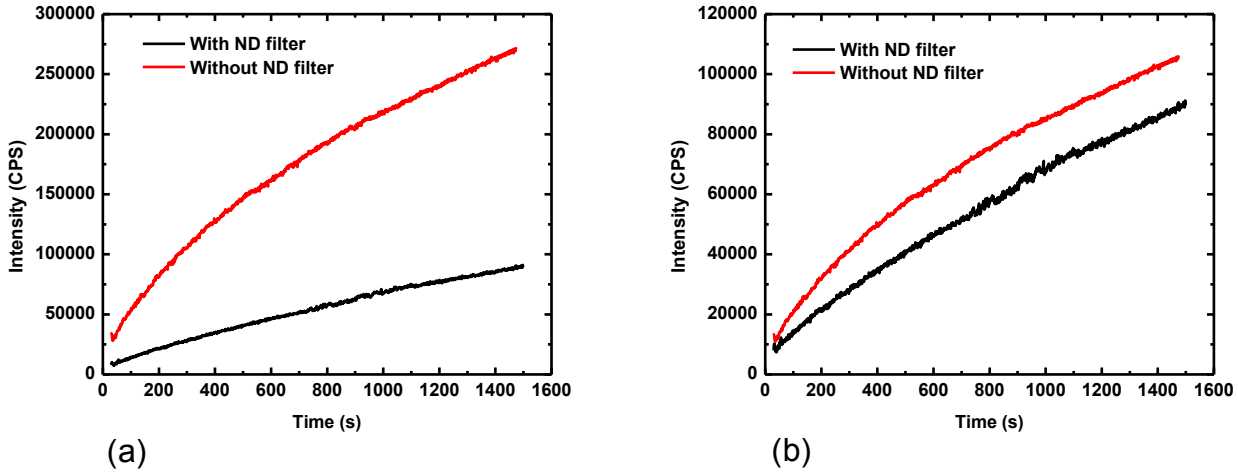

Figure 3.16 Fluorescence kinetic traces of (a) oxidation observed under air for a 2.88 ppm AQU/*n*C_{60} sample with and without neutral density filter and (b) same data as in (a), but red curve multiplied by 0.39

Condition	$[C_{60}]$ (ppm)	k_1 ($M^{-1}s^{-1}$)	k_2 ($x10^5$) ($M^{-1}s^{-1}$)	$[A_4]$ ($x10^{-8}$) (M)	$k_2x[A_4]$ ($x10^{-4}$) (s^{-1})	Coefficient ($x10^{12}$)
	2.88					
Without neutral density filter						
Air		803	0.335	1.72	5.76	3.08
Nitrogen		546	1.130	0.52	5.88	5.12
Oxygen		449	0.710	0.55	3.87	4.64
With neutral density filter						
Air		717	3.740	0.52	19.4	1.20
Nitrogen		220	0.810	0.80	6.48	2.00
Oxygen		222	1.800	0.68	12.2	1.81

Table 3.4 Rate constants obtained with and without neutral density filter for 3 different atmospheric conditions

If photo induced oxidation occurred in this system, the rate constants obtained in the presence of a neutral density filter must be smaller. And also in the absence of photo induced oxidation the rate constants calculated with and without neutral density filter must be the same. As seen in Table 3.4 in all three cases of air, nitrogen and oxygen the k_1 being consistently slower in the presence of the filter, suggested that photo induced oxidation is possible.

When comparing the effect of modified atmospheres on oxidation, the k_1 data shown at each atmospheric condition didn't correlate as expected. If oxygen was participating in one of the

oxidation steps, presence of oxygen in the reaction medium should have increased the rate of reaction and thus increased the rate constants.

3.4 Conclusions

The present study revealed that, contrary to conclusions by much of the scientific community,[36, 38-41, 43-45] AQU/*n*C_{60} suspensions are indeed acting as oxidants, and that the rate of oxidation had a direct relationship with the concentration of C_{60} present in the suspensions. We have demonstrated a reproducible, high-sensitivity experimental and analytical method for monitoring the oxidation and have illustrated its use with a simplified kinetic model that consists of a pair of parallel oxidative steps. The results of the modeling are not consistent across multiple sample conditions, and thus will need to be revised in future work to better match the experimental data.

CHAPTER IV

THERMAL STABILITY OF nC$_{60}$ COLLOIDAL SUSPENSIONS

4.1 Introduction

The formation of extremely stable colloidal aggregates that are colloidally stable for months by supposedly hydrophobic C_{60} nanoparticles has been highlighted in a number of reports.[9, 13, 15, 25, 26] The propensity of fullerenes to self-aggregate under aqueous conditions and the factors influencing this aggregation have direct consequences for the environmental and physiological behavior of these materials, including their reactivity and environmental health and safety issues. The effect of temperature on these colloids plays a significant, but as-yet understudied role in both the synthesis and reactivity of these systems in addition to many other, better-studied parameters including pH, ionic strength, and the presence of dissolved organic acid. All of these parameters may be intimately related to aggregation state, which in turn may be a vital factor in determining bioavailability as well as reactivity.[25] In addition to the effect on aggregation reported previously, an initial observation in our laboratory revealed that temperature affects the TTA/nC$_{60}$ (described in Chapter 2) synthesis procedure, resulting in C_{60} sedimenting out of suspension at or near 50 °C in the rotary evaporation step. Given that the colloids are mainly composed of C_{60} and $C_{60}O$, this observation led us to hypothesize that $C_{60}O$ might play a significant role in stabilizing the colloid hence increasing the temperature might cause thermally-

activated reaction with $C_{60}O$ which in turn de-stabilize the colloids. The main thermal reaction of $C_{60}O$ reported in literature is the formation of $C_{120}O$ with C_{60}[69, 70] as shown in Figure 4.1.

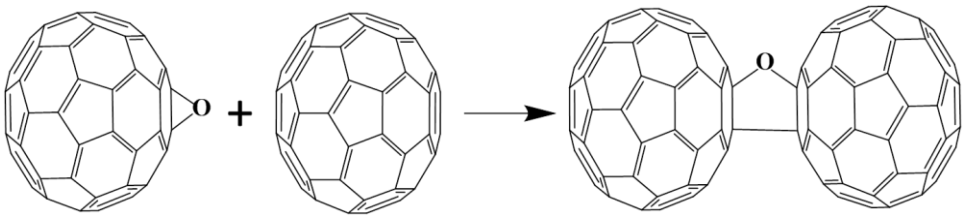

Figure 4.1 Formation of $C_{120}O$ from C_{60} and $C_{60}O$

As reported, the synthesis of this bridged dimer $C_{120}O$ in significant quantities requires higher temperatures around 180-200 °C, but this transformation can also take place spontaneously upon storage.[87, 88] The nature of this thermal dependence or the thermally-activated transition has not been fully explored in reported literature.

This chapter discusses some of the initial attempts taken to investigate the thermal stability of these colloids prepared by all four primary *n*C_{60} synthesis methods (described in Chapter 2). If the identified dimerization reaction takes place when heating the colloid, the oxygen atoms, so central to stabilizing the colloid in an aqueous system, would become significantly less accessible to accept hydrogen bonds from the aqueous medium, thereby explaining the apparent drop in observed colloid stability. To test our hypothesis thermally treated colloidal suspensions have been analyzed for $C_{120}O$ or further polymerized products of C_{60} ($(C_{60})_xO_y$) using HPLC along with visual observations. Furthermore, thermally treated samples that have been precipitated from suspension have also been analyzed for any detectable products mentioned above.

4.2 Results and Discussion

Based on our laboratory observations and the hypothesis discussed above we would expect the colloids to sediment out of suspension upon increasing the temperature. According to visual observations none of the colloidal suspensions prepared by AQU/nC$_{60}$, SON/nC$_{60}$, THF/nC$_{60}$ and TTA/nC$_{60}$ methods showed any noticeable sedimentation or precipitation.

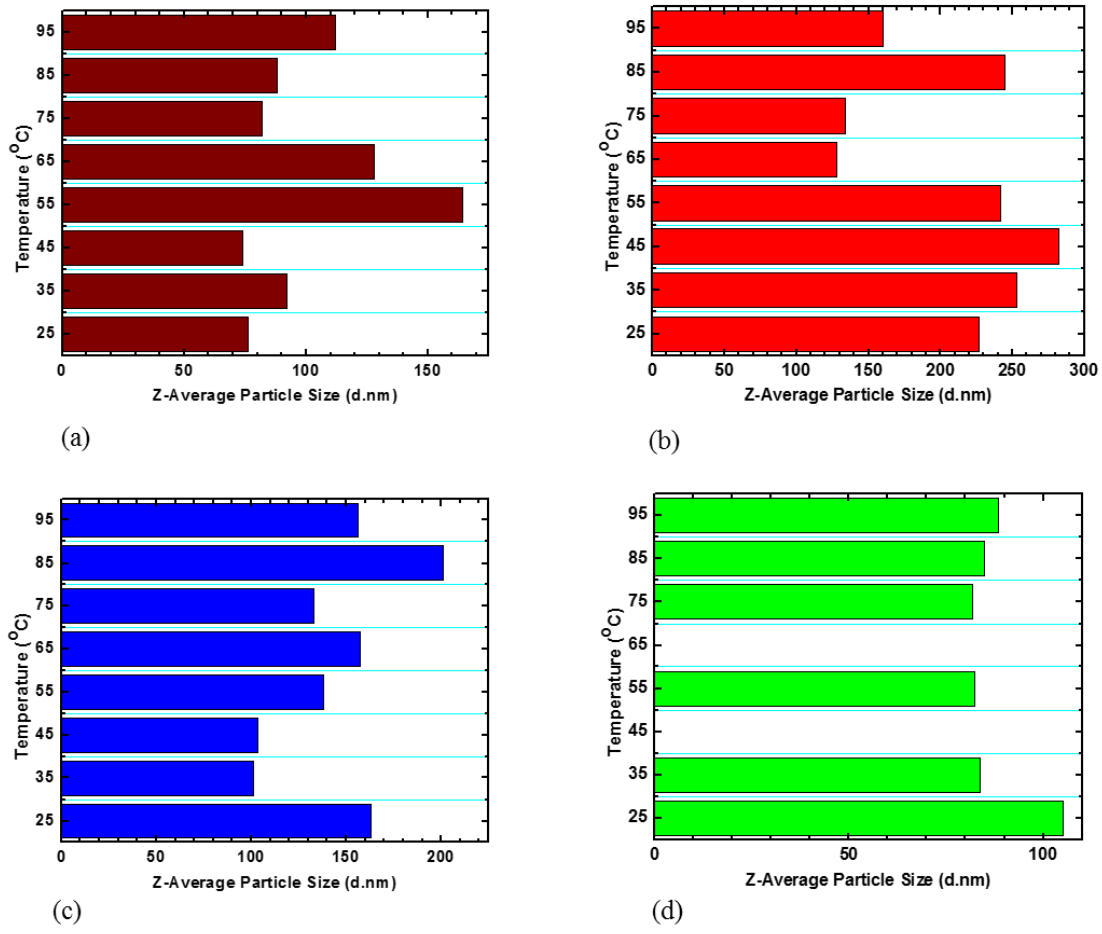

Figure 4.2 Z-Average particle size for (a) AQU/nC$_{60}$, (b) SON/nC$_{60}$, (c) THF/nC$_{60}$ and (d) TTA/nC$_{60}$ at temperatures from 25-95 °C

Figure 4.2a, 4.2b, 4.2c and 4.2d shows the dynamic light scattering data for aqueous colloidal suspensions prepared by AQU/*n*C_{60}, SON/*n*C_{60}, THF/*n*C_{60} and TTA/*n*C_{60} methods, respectively, at every temperature extracted during the thermal stability test. For a given sample, the Z-Average particle sizes observed at each temperature did not vary much compared to the particle size ranges reported in literature.[89] Even though particle size information did not show us huge variations with each temperature, these data were not sufficient to draw definitive conclusions about aggregation or sedimentation occurring in the suspensions.

Previous work reported by Murdianti *et al*.[31] demonstrated that $C_{60}O$ present at the surface of the *n*C_{60} particles was sufficient enough to produce stable colloidal suspensions in water in AQU/*n*C_{60} samples. Thus, $C_{60}O$, being the dominant hydrophilic surface component of these colloidal suspensions, a thermally activated transition, such as conversion to $C_{120}O$, is shown in Figure 4.1 will bury the hydrophilic component, resulting in less hydrophilicity on the colloidal surface that might induce crashing. In accordance with this report and assuming our initial hypothesis was correct, if enough $C_{60}O$ was present on the surface of the colloids, we should have observed visual crashing or precipitation of the suspensions made by AQU/*n*C_{60} samples. However, the observation that these colloids were stable for up to 98-100 °C suggested that we might not have had high enough concentrations of $C_{60}O$ present in the colloid to be able to visually observe the crashing.

An AQU/*n*C_{60} sample made from deliberately enriching it with $C_{60}O$ was investigated for its thermal stability using the same procedure discussed in Chapter 2, section 2.4. Crashing out of suspension or precipitation was not visually apparent. To further verify this observation, HPLC analysis was carried out using the suspension resulting from thermal treatment, to evaluate the appearance of $C_{120}O$ in the chromatogram that might have formed during the thermal treatment. The specific retention time for $C_{120}O$ was recorded in a separate chromatogram using, an independently synthesized sample of $C_{120}O$, under the same chromatographic experimental

conditions. Figure 4.3 shows the chromatogram obtained for the thermally treated sample, and the chromatogram in Figure 4.4 shows the retention time for $C_{120}O$.

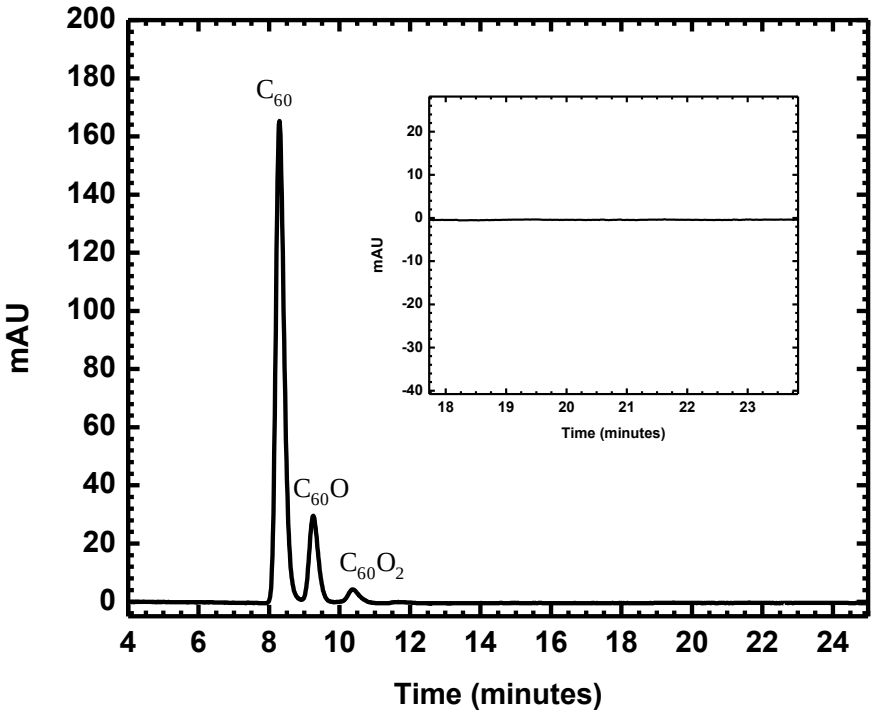

Figure 4.3 HPLC chromatogram of thermally treated AQU/*n*C_{60} sample enriched with $C_{60}O$

As evident from the chromatogram (Figure 4.3), there was no peak apparent around 20-22 min retention time in the thermally treated $C_{60}O$ enriched sample, suggesting there might not be any thermally activated transitions taking place in the suspension which could be accountable for the crashing.

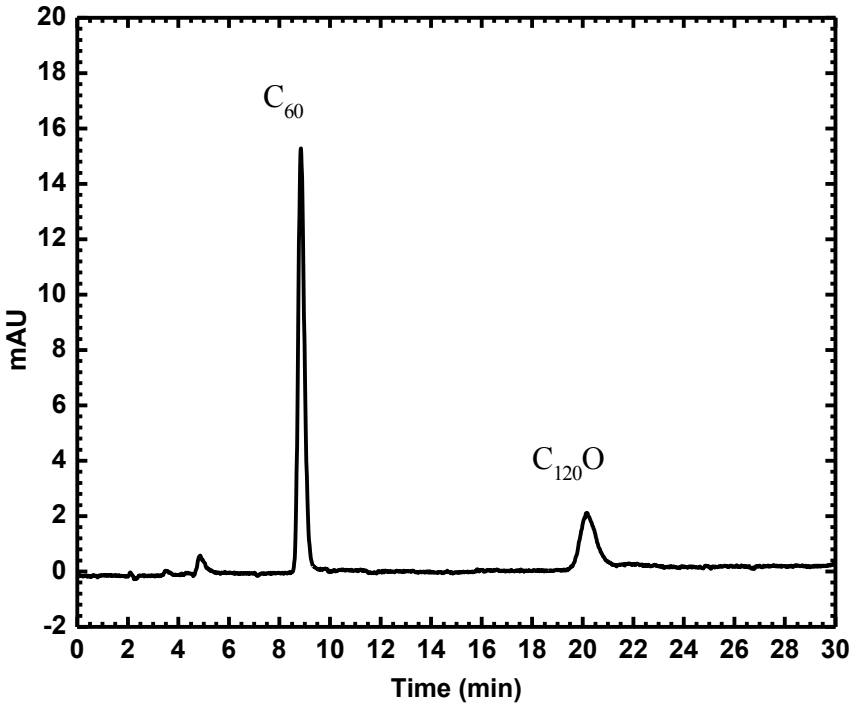

Figure 4.4 HPLC chromatogram for $C_{120}O$

In order to test the effect of rotary evaporation on crashing, an experiment was carried out in a rotary evaporator. A sample was heated at a 60 mbar reduced pressure at 65 °C, deliberately concentrating the sample while heating. The heating was carried out until dryness. The dried solid was collected and analyzed for $C_{120}O$ using HPLC to determine whether or not a deliberate drying down (while concentrating) might induce the formation of $C_{120}O$. Figure 4.5 shows a chromatogram obtained for the dried down solids which were re-dissolved in toluene. Compared to the standard $C_{120}O$ chromatogram showed in Figure 4.1, there is no identifiable $C_{120}O$ peak shown in the chromatogram (Figure 4.5). Figure 4.6 shows a chromatogram collected on the same sample showed in Figure 4.5, but for a longer time as an attempt to observe any polymeric C_{60} species that might appear in the sample.

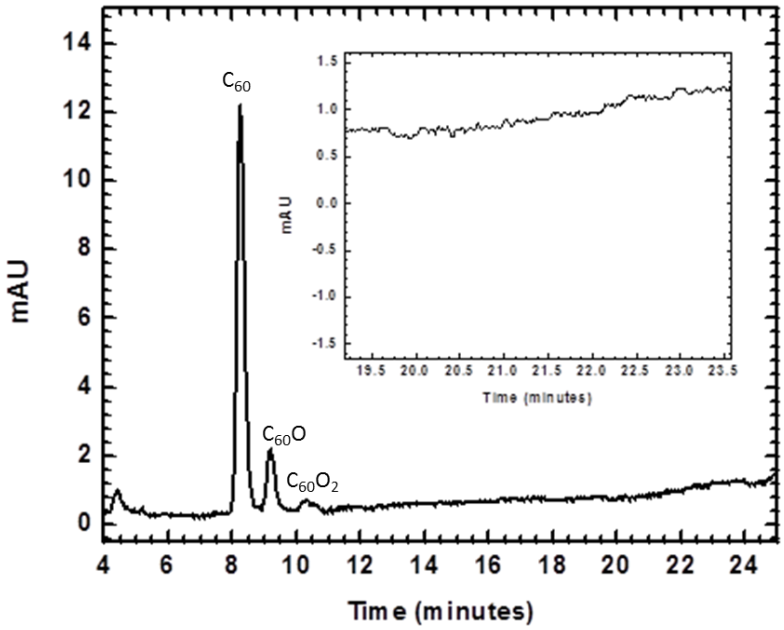

Figure 4.5 HPLC chromatogram of deliberately dried solids using rotary evaporation and re-dissolved in toluene

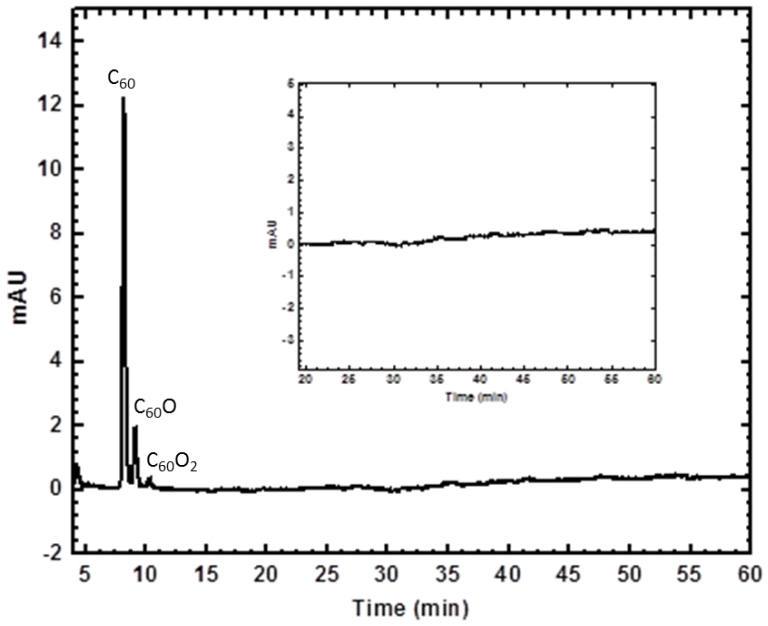

Figure 4.6 HPLC chromatogram showing longer time data collected on deliberately dried solids using rotary evaporation and with the solids re-dissolved in toluene

However, there is no appearance of $C_{120}O$ or any other polymeric species as evident from the chromatogram in Figure 4.5. These data confirmed that even under deliberate concentrating conditions applied to AQU/*n*C_{60}, the initially hypothesized transformation was not occurring. Hence AQU/*n*C_{60} suspensions are stable up to about 98-100 °C.

4.3 Conclusions

The proposed hypothesis for the observed crashing of *n*C_{60} suspensions was disproved. All the suspensions were thermally stable up to about 98-100 °C based on visual observations. Further experimentation on AQU/*n*C_{60} confirmed that there was no thermally activated transformation occurring during heating in a water bath or rotary evaporation conditions as evident by HPLC analysis. While the initial attempts disproved the hypothesis of the formation of $C_{120}O$, additional experiments are needed using higher concentrations and other *n*C_{60} synthesis methods to verify the conclusions drawn in this chapter and to assess alternate explanations for the observed instability of these samples via rotary evaporation.

CHAPTER V

FULLERENE COLLOID CONCENTRATION DETERMINATION: METHOD DEVELOPMENT

5.1 Introduction

No fundamental property measurement is more central to kinetic studies, hazard evaluation, and standardized procedure development than is concentration determination. This measurement is strikingly difficult for fullerenes, particularly in their aqueous colloid forms. Gravimetric methods are significantly difficult because the solid as-received materials contain residual solvent molecules in ill-defined clathrate structures.[72] Colloids of fullerenes are not amenable to Beer's Law-based absorption determination of concentration because of particle-size-dependent scattering and because of the appearance of a pseudo-solid-state absorption band that overlaps the main diagnostic absorption peak. Extraction into organic solvents often results in solutions of mixtures due to environmentally-induced changes, such as oxidation by ozone,[31] that have different absorption spectra that make Beer's Law application to the extracts problematic.

According to literature reports, UV/Vis absorbance has been used to determine concentration and extraction efficiency of fullerenes.[12, 13, 15, 37, 76, 90-92] We have adapted the procedure described by Deguchi[15] which involves salting out of aqueous fullerene colloids into toluene to yield complete extraction and then fitting the experimental absorbance curve to a

calibrated reference spectrum of C_{60} in toluene according to Beer's law to calculate the concentrations.

However, differences in concentrations have been observed when comparing samples that were subjected to stirring and sonication during the extraction procedure as well as upon drying and not drying the toluene layer with Na_2SO_4 (detailed procedure for concentration determination was discussed in section 2.2.3). Furthermore, in some of our experiments inability to fit the reference spectrum data with experimental data has been observed, where accurate concentration determination could not be done. Figure 5.1a and 5.1b shows two examples where in 5.1b, experimental absorbance curve was adequately fitted with the standard calibrated reference spectrum of C_{60} in toluene in order to calculate the concentration. However in Figure 5.1a, failure to obtain adequate fitting suggested the necessity of more accurate methods.

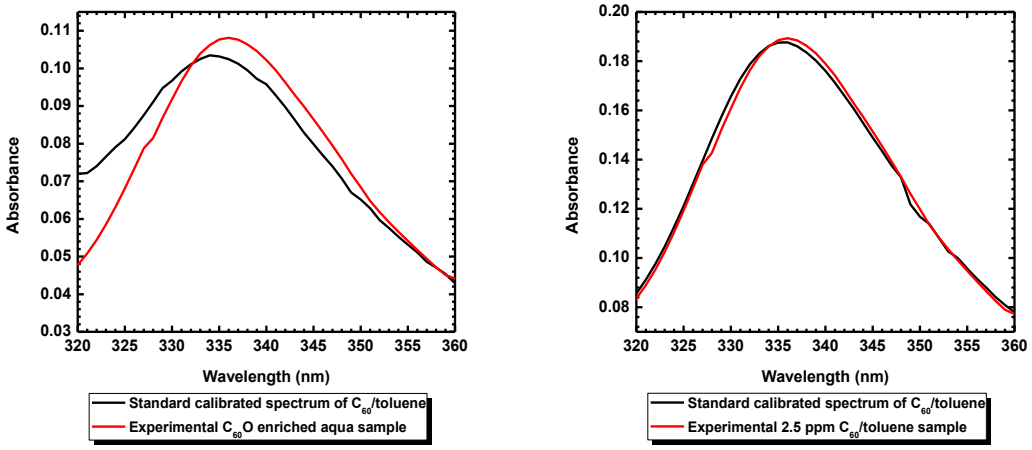

(a) (b)

Figure 5.1 Experimental UV/Vis absorbance curves (a) $C_{60}O$ enriched AQU/*n*C_{60} sample, (b) 2.5 ppm C_{60}/toluene, which were fitted to a standard calibrated spectrum of C_{60}/toluene

Unlike solutions of C_{60} dissolved in organic solvents, such as toluene and tetrahydrofuran, where extinction coefficients are useful in determining concentrations according Beer's law, for colloidal suspensions of C_{60}, simply using an extinction coefficient is not

sufficient due to two reasons. In an absorbance measurement colloids will not only absorb light but will also scatter light in different amounts depending on the size of the particles present in the suspension, resulting in complications in the absorbance measurements. In C_{60} suspensions, there is a broad pseudo solid state absorption band occur at 400-500 nm[11] that overlaps with the main absorption band at 336-337 nm, the relative size of which will depend on the size of the particles present in the suspension, which again makes the absorbance measurement difficult. Thus, there was a need to develop a good method of extraction and concentration determination of these colloids.

This Chapter describes a HPLC gravimetric calibration curve method that was developed for the accurate determination of concentrations of C_{60} compared to the UV/Vis spectroscopic method.

5.2 Results and Discussion

The HPLC chromatograms obtained for the six gravimetric standard solutions of C_{60} in toluene (1, 2.5, 5, 10, 20 and 50 ppm) and their corresponding UV/Vis spectra showed the characteristic absorbance at 336 nm in Figures 5.2 and 5.3.

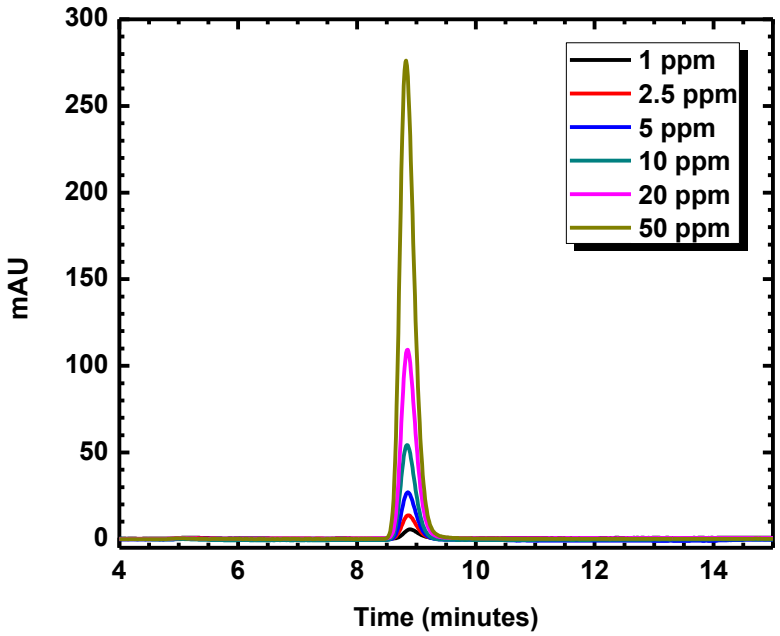

Figure 5.2 HPLC chromatograms of gravimetric standard solutions of C_{60} in toluene

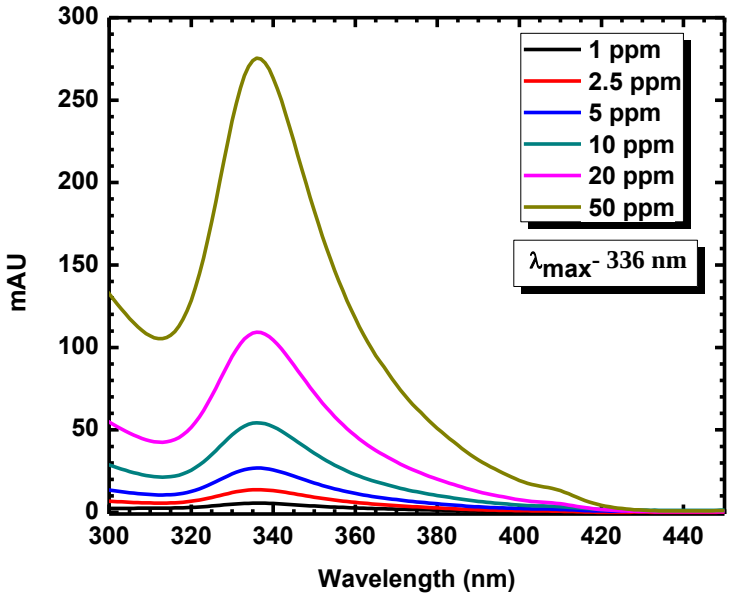

Figure 5.3 UV/Vis absorbance spectra of gravimetric standard solutions of C_{60} in toluene

To construct the HPLC calibration curve, the peak corresponding to C_{60}, which was eluted around 9 minutes in each chromatogram shown in Figure 5.2, was integrated using the HPLC Galaxie™ Chromatography Workstation to calculate the peak areas. The calibration curve shown in Figure 5.4 was obtained by plotting peak areas versus corresponding gravimetric C_{60} concentrations. Using OriginPro 8 software, a linear fit for the data points was obtained, and the slope of the calibration curve was 1.62. The equation obtained for the calibration line is shown in the graph, where *y* is the peak area at the corresponding concentration of *x*.

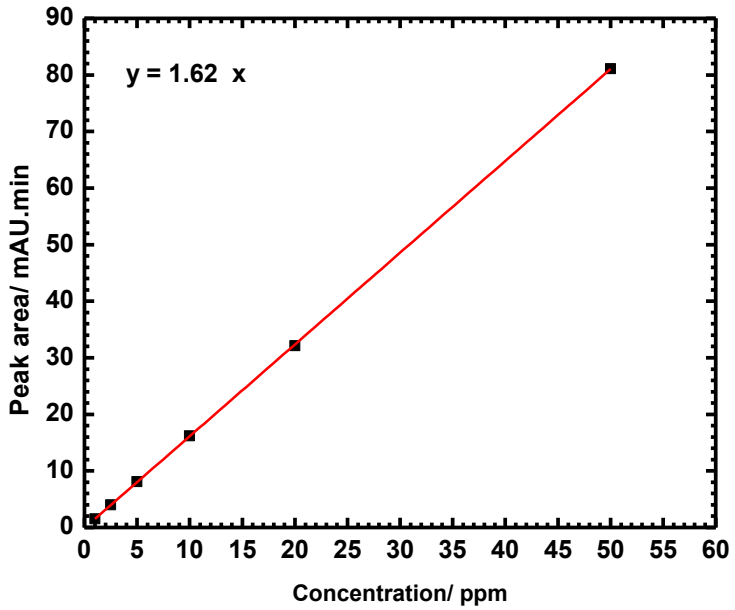

Figure 5.4 Calibration curve for the gravimetric C_{60} standard solutions

As explained in Chapter 2, section 2.5.1, another calibration curve was constructed using three gravimetric standard solutions of C_{60} in toluene (1, 5 and 20 ppm) which were initially stirred with water before analyzing via HPLC. Due to the concentration differences observed in dried and not dried toluene layers that were analyzed by UV/Vis spectroscopy, this set of data

was obtained to determine if there was an effect by water that caused a difference in concentration while extracting C_{60} from aqueous colloidal suspensions into toluene. Figure 5.5 shows a HPLC chromatograms obtained for those three gravimetric standard solutions of C_{60} in toluene, and their corresponding UV/Vis spectra showing the characteristic absorbance at 336 nm are shown in Figure 5.6.

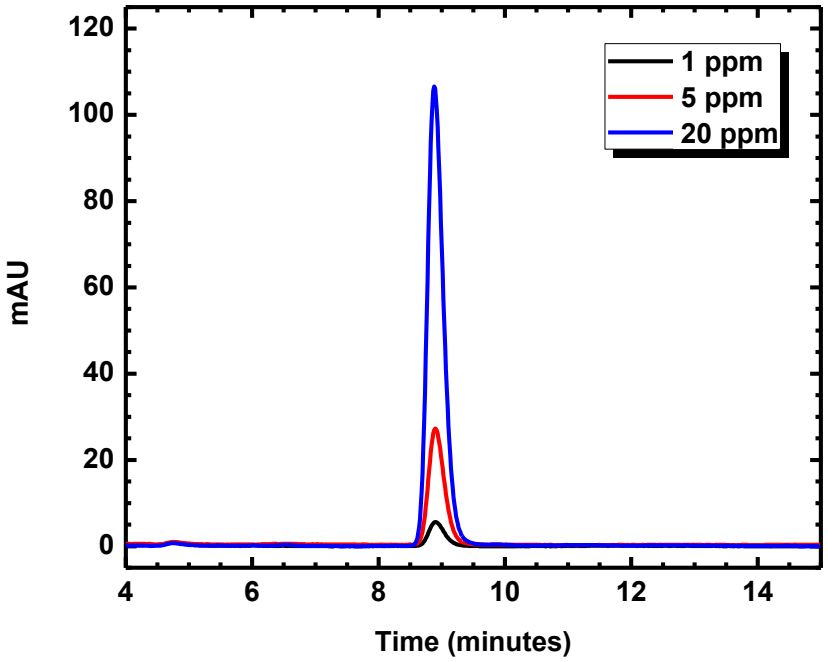

Figure 5.5 HPLC chromatograms of the gravimetric standard solutions of C_{60} in toluene which were initially mixed with water

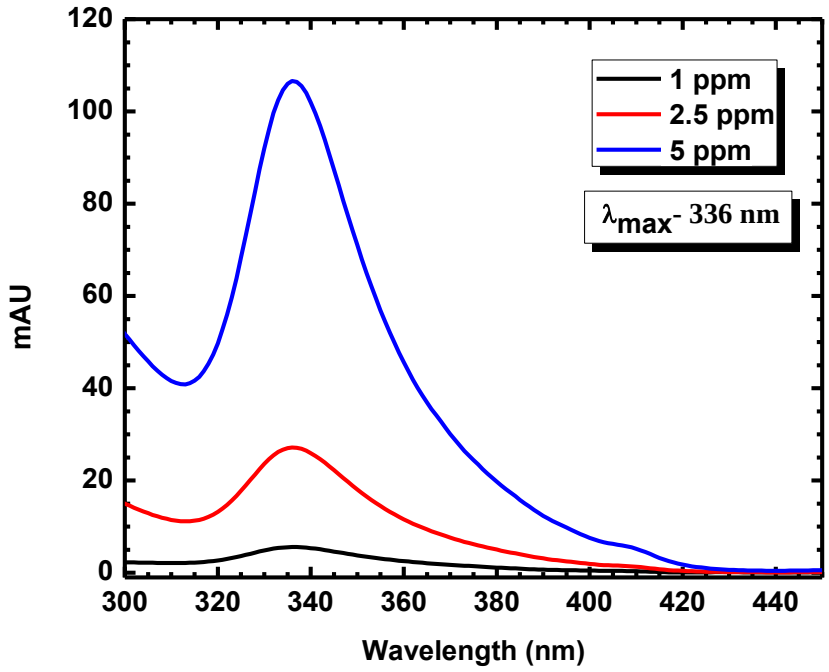

Figure 5.6 UV/Vis absorbance spectra of gravimetric standard solutions of C_{60} in toluene which were initially mixed with water

The calibration curve for these samples was obtained in the same manner by using HPLC Galaxie™ Chromatography Workstation to calculate the peak areas. The calibration curve shown in Figure 5.7 was obtained by plotting peak areas versus corresponding gravimetric C_{60} concentrations. OriginPro 8 software was used to obtain a linear fit for the data points, and the slope of the calibration curve was 1.58. The equation obtained for the calibration line is shown in the graph, where *y* is the peak area at the corresponding concentration of *x*.

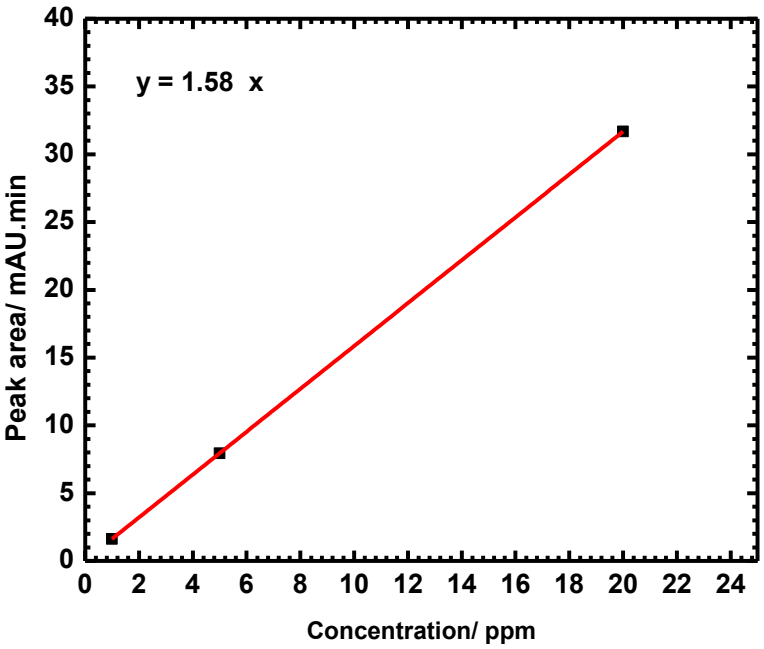

Figure 5.7 Calibration curve for the gravimetric C_{60} standard solutions

As seen from the two calibration curves, their slopes calculated from the linear fits were nearly the same. This observation suggested that extracting toluene over an aqueous phase should not affect its final measurement of concentration.

Table 5.1 shows a summary of concentration data calculated from both methods, HPLC calibration curve method and UV/Vis spectroscopic method using a calibrated C_{60}/toluene spectrum, for a C_{60}/toluene sample that had original gravimetric concentration of 5 ppm.

Sample	Concentration/ ppm		
	HPLC	UV/Vis	
		From dried toluene layer	From not dried toluene layer
5 ppm C_{60}	5.54	-	5.58
5 ppm C_{60} mixed with water	5.48	5.76	5.74
5 ppm C_{60} mixed with water and $NaNO_3$	5.54	5.85	5.66
5 ppm C_{60} sonicated with water	5.23	5.90	5.75
5 ppm C_{60} sonicated with water and $NaNO_3$	5.48	5.96	5.79

Table 5.1 Summary of HPLC and UV/Vis concentration data for a 5 ppm C_{60}/toluene sample that had undergone different treatment conditions prior to the concentration determination

Figure 5.8 shows the HPLC chromatograms of corresponding C_{60} solutions in toluene which were prepared under different process conditions prior to HPLC analysis as shown in Table 5.1. Concentration data recorded from the HPLC method was obtained using respective peak areas of each sample.

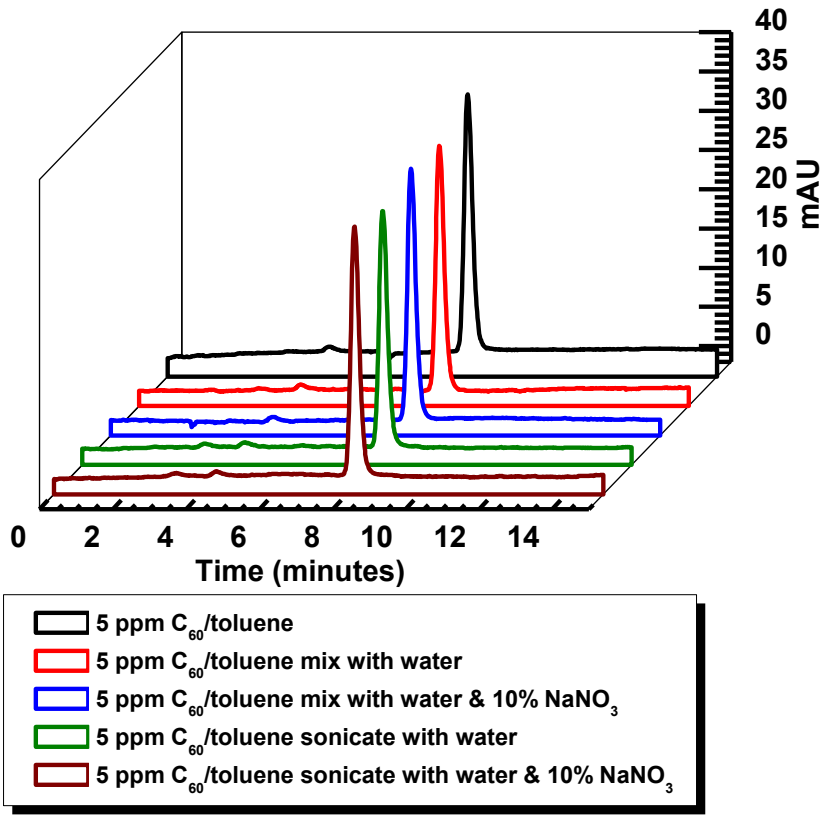

Figure 5.8 HPLC chromatograms of 5 ppm C_{60} dissolved in toluene which were prepared under different process conditions prior to HPLC analysis

A few examples showing the experimental UV/Vis absorbance curves achieved for the same set of samples which were fit to a standard calibrated spectrum of C_{60} dissolved in toluene were shown in Figure 5.9a, 5.9b, and 5.9c.

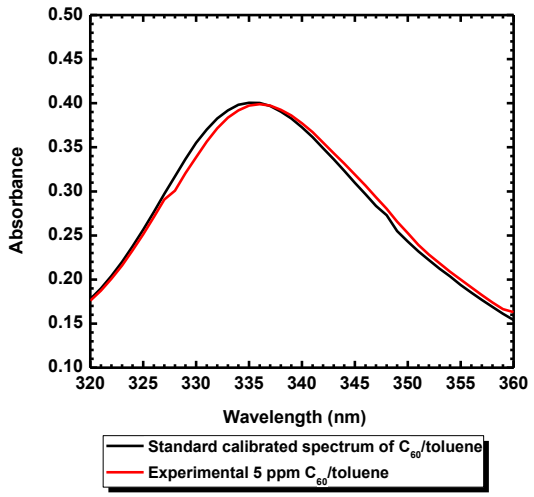

(a)

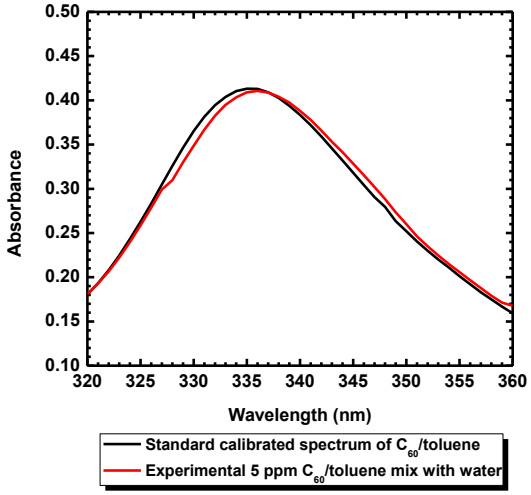

(b)

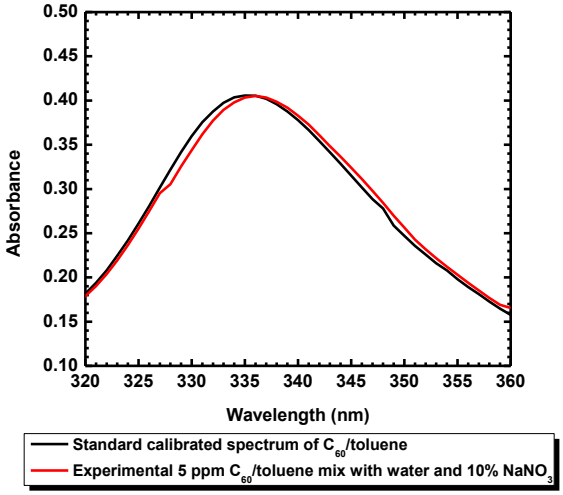

(c)

Figure 5.9 Experimental UV/Vis absorbance curves (a) 5 ppm C_{60}/toluene, (b) 5 ppm C_{60}/toluene mix with water and (c) 5 ppm C_{60} mix with water and 10% $NaNO_3$, which were fitted to a standard calibrated spectrum of C_{60}/toluene

Concentration data recorded in Table 5.1 from UV/Vis method was obtained via fitting to a standard calibrated spectrum of C_{60}/toluene for each sample. As evident from Figures 5.9 a-c,

the spectra do not fit perfectly, suggesting that the concentration values drawn from that method might not be accurate.

Compared to the original gravimetric concentration of C_{60}, which was 5 ppm, both analysis methods gave reasonable data, but compared to the UV/Vis data, the HPLC data were more consistent and accurate.

5.3 Conclusions

The HPLC calibration curve method was more useful in calculating concentrations of unknown C_{60} solutions over UV/Vis spectroscopic procedure. Thus, this method was chosen as the standard operating procedure for concentration determinations.

CHAPTER VI

C_{60}–POLYMER NANOCOMPOSITE NETWORKS ENABLED BY GUEST–HOST PROPERTIES

6.1 Introduction

A recent work reported by Gyanwali *et al.*[68] demonstrated that inclusion complexes of non-covalently bound linear polymer chains of polypropylene oxide in cyclodextrin (CD) networks exhibited interesting physical, swelling, and sequestration properties. Early literature reports on cyclodextrin inclusion complexes revealed that fullerenes are a great candidate for inclusion due to its hydrophobicity and comparable size for the inner cavity of γ-cyclodextrin.[93, 94] Moreover, fullerenes have been of potential interest among the scientific community to synthesize nanocomposites with linear, branched or networked polymers to enhance mechanical,[50-53] electronic[54] and photosensitization[55-59] properties, among others. Furthermore, possibility of encapsulating fullerenes within a polymeric form of cyclodextrin raises the possibility of using such a structure to sequester fullerenes, thereby mitigating their potential environmental, health and safety concerns.

This chapter describes a method for encapsulating C_{60} in an engineered cross-linked polymer network formed from γ-CD and dodecyl chains. A simple synthesis route is presented to achieve thin membranes/films of homogeneously intercalated C_{60} in the polymer network. These

composites were found to maintain a stable C_{60} concentration in the network, presumably via van der Waals guest−host interactions within the hydrophobic γ-cyclodextrin cavity. The research presented in this chapter is published in the journal *Macromolecules*.[95]

6.2 Method Development

The γ-cyclodextrin network synthesized by our collaborator Dr. Gaumani Gyanwali, was achieved by chemically cross-linking individual cyclodextrin units with bifunctional hexamethylene chains, and this network showed interesting swelling and sequestration properties.[67] There were three main requirements that should be satisfied by the solvent chosen for the study in order to achieve better C_{60} incorporation such as a solvent that is capable of swelling the network polymer, dissolve C_{60} and, more specifically, did not dissolve C_{60} so well that might avoid C_{60} being incorporated into the CD. Therefore, selecting a suitable solvent under the restrictions stated above was thoroughly investigated. Toluene was well known for solubilizing C_{60} to achieve individual fullerene molecules,[96] and thus it was selected as the first trial solvent for both the network polymer and C_{60}. γ-Cyclodextrin/dibromohexane polymer network was not adequately swelled even after overnight stirring with toluene and with additional stirring for about 5 hours in a water bath at 60 °C, sufficient amount of swelling was observed. To ensure complete swelling of the network, the stirring was continued for another night without heating. The clear/cloudy suspension of swelled polymer was then added to a C_{60}/toluene solution, and the mixture was heated for another hour at 60 °C. The cooled down mixture was then filtered through vacuum filtration using Whatman® filter, and the resulted film was washed with 3 aliquots of 10 mL DMF. The resulted film showed no evidence of encapsulated C_{60} and

was pale whitish with few spots with faint black colour which may be due to C_{60}. However, most of the C_{60} was not sequestered and ended up in the filtrate suggesting that, using a "good" solvent (toluene) to solubilize C_{60} may prevent it from encapsulation due to its preference to remain in the solvent rather than in the network.

In response to the above observation, a variety of solvents were tested against the cyclodextrin network and C_{60}, and included hexane, N,N-dimethylformamide (DMF), dimethylsulfoxide (DMSO), 2-pentanol, benzonitrile, benzaldehyde, 1-pentanol, 2-pentanol, 1-hexanol and 1-bromopropane. None of the solvents, except DMF, worked with at least one of the two components, the C_{60} or the network to achieve good solubilization or swelling respectively. DMF and DMSO showed sufficient amount of swelling of the polymer network upon stirring, but DMSO did not show adequate solubility of C_{60}. Moreover, binary solvent systems consisting of toluene and acetonitrile were also tried. The films were prepared using the binary solvent consisting of different volume ratios of the two solvents such as, 1:3, 2:3 and 10:1 acetonitrile:toluene. Additionally, some films were prepared by the gradual addition of acetonitrile into a solution of C_{60}/cyclodextrin network dissolved in toluene. The films prepared from the binary solvent system showed sufficient amount of captured C_{60} (evident from their color), but were not stable for additional toluene washing steps and tended to lose most of the C_{60} during washing. This suggested that most of the C_{60} was not encapsulated but just deposited on the membrane.

Consequently, DMF was chosen as the solvent to further study the C_{60} encapsulation. Considering the size of a fullerene molecule and, the tie chain length between cyclodextrin moieties present in the network, dibromododecane rather than dibromohexane was chosen as the bifunctional reagent to synthesize the new networks with longer tie chain lengths. γ-Cyclodxtrin/dibromododecane network sysnthesis was achieved by Gaumani Gyanwali & Mathis Hodge, in Dr. Jeffery White's research group. By synthesizing this new network material, we

expected to increase the accessibility of fullerenes into cyclodextrin moieties present in the network.

6.3 Results & Discussion

The membranes prepared only from γ-CD/dibromododecane polymer network according to the procedure discussed in section 2.6.1 in Chapter 2 are shown in Figure 6.1.

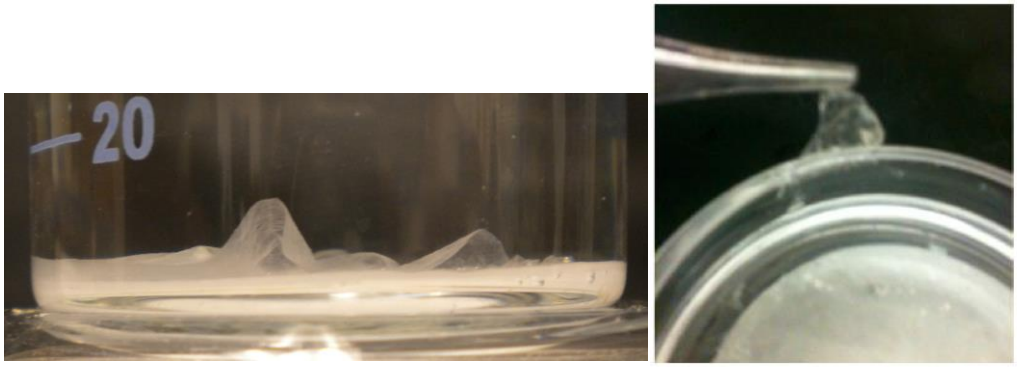

a. **b.**

Figure 6.1 γ-CD/dibromododecane membrane, a) dipped in DMF, b) piece of membrane torn apart while pulling out of the solvent

Figure 6.1a shows a translucent membrane on the filter paper which was dipped in DMF after vacuum filtration and a subsequent overnight drying step carried out during the synthesis. Figure 6.1b illustrates removal of the same membrane from the solvent using a pair of forceps. As seen in the picture the membrane was extremely fragile and was torn apart during efforts to remove it from the solvent and actually curled up.

Figure 6.2a depicts the C_{60}-intercalated membrane dipped in DMF along with the filter paper after the vacuum filtration and subsequent overnight drying steps. As seen in the picture, the membrane was completely swelled in DMF within ~30 seconds, resulting in a so called "jelly fish" type appearance.

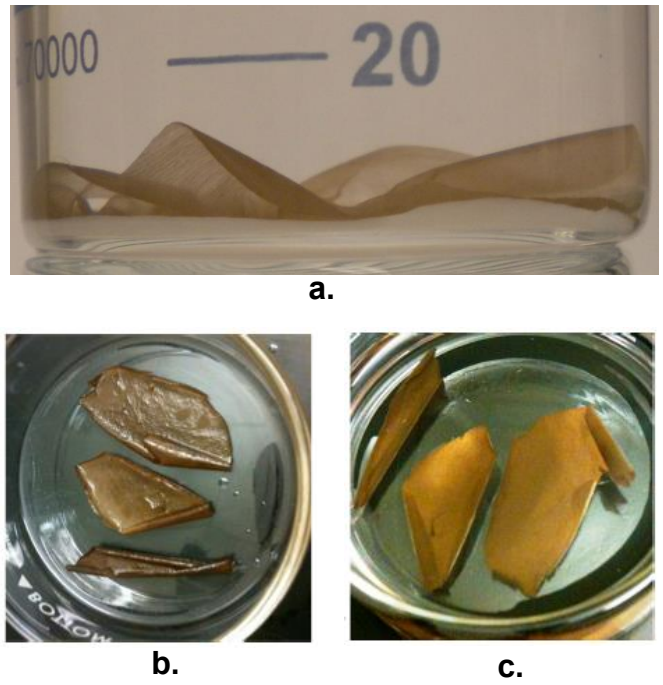

Figure 6.2 C_{60}/γ-CD/dibromododecane membrane, a) dipped in DMF, b) placed in a dry container after removal from DMF and c) the same membranes obtained after six separate 24 h washings in toluene

Compared to γ-CD/dibromododecane membranes, C_{60}-intercalated membranes were uniformly brown in color, indicating even distribution of C_{60} molecules throughout the membrane. Unlike γ-CD/dibromododecane membranes, C_{60}-intercalated ones had sufficient structural integrity and toughness to be able to easily pulled off of the filter paper. Figure 6.2b shows the dried membranes which were taken out of DMF, and, as evident from the picture, these tend to curl-up to some extent from the edges. Figure 6.2c illustrates the same membranes

obtained after 6 separate 24-h washings in toluene in a shaker bath. Observations of the homogeneity of C_{60} distribution and intact membranes suggested the stability of these membranes was due to the presence of well distributed C_{60} that has been encapsulated with in cyclodextrin moieties in the network, which cannot be easily removable even with toluene which is an excellent solvent for C_{60}. Additionally these membranes were stable in acetone and, as expected, didn't show any swelling or wetting in water.

As shown in Figure 6.3, the nature and quantity of C_{60} left in toluene washing fractions were analyzed by UV/Vis spectroscopy. For comparison purposes, toluene washings of a membrane prepared by C_{60}/γ-cyclodextrin/dibromohexane (6.3a) during the method development process and C_{60}/γ-CD/dibromododecane membrane (6.3b) were shown. Membranes prepared from C_{60}/γ-CD/dibromohexane networks were continuously losing C_{60} even after twelve wash cycles as demonstrated from the 336 nm peak in the UV/Vis spectrum of Figure 6.3a. This suggests mostly un-intercalated C_{60} may be due to restrictions caused by inadequate tie chain length between cyclodextrins. In contrast, membranes of C_{60}/γ-CD/dibromododecane showed no evidence of C_{60} being removed after six wash cycles. This observation, in combination with homogenous distribution of C_{60} in still intact membranes as shown in Figure 6.2c, provided strong evidence for C_{60} intercalation. Attempts to record UV/Vis spectral data of the membranes failed because the membranes were opaque.

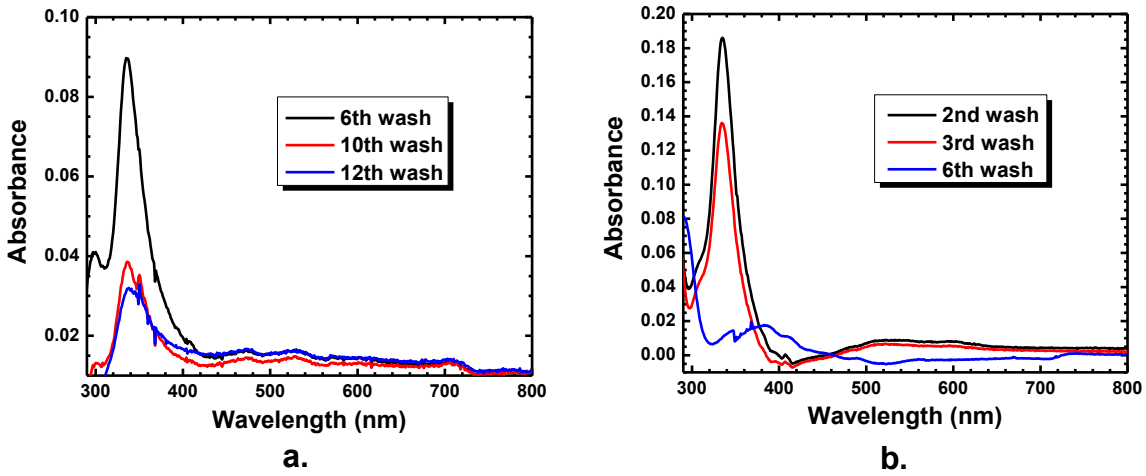

Figure 6.3. UV-Vis spectroscopy results for toluene extracts as a function of the number of extractions, a) C_{60}/γ-CD/dibromohexane and b) C_{60}/γ-CD/dibromododecane

This conclusion was further confirmed by ^{13}C solid-state MAS NMR spectra, (produced by Gaumani Gyanwali & Mathis Hodge, in Dr. Jeffery White's research group) where calculations showed 66% of the original C_{60} content remained in the membrane. The $\%C_{60}$ left after each step, calculated from quantitative analysis of the peak areas resulted from ^{13}C solid-state MAS NMR spectra, were shown in table 6.1 (adapted from *Macromolecules* **2013,** 46, (15), 6118-6123).[95]

Sample	$\%C_{60}$ remaining
Original mixture of C_{60} and γ-CD network	100
"As prepared" membrane	91
Membrane after 3rd wash	73
Membrane after 6th wash	66

Table 6.1: The $\%C_{60}$ left after subsequent washing steps as compared to the original mixture[95]

A plot of the number of washing steps versus % C_{60} remaining is shown in Figure 6.4. As shown by the fitting curve an offset exponential decay model fitted the data extremely well, and the vertical offset fit gave the asymptotic incorporation level (presumably the bicapped fullerene content) to be 60%. The asymptotic incorporation level calculated from the fit was almost similar to the % C_{60} which remained after final wash step as quantified by ^{13}C NMR studies, which further confirmed our incorporation level.

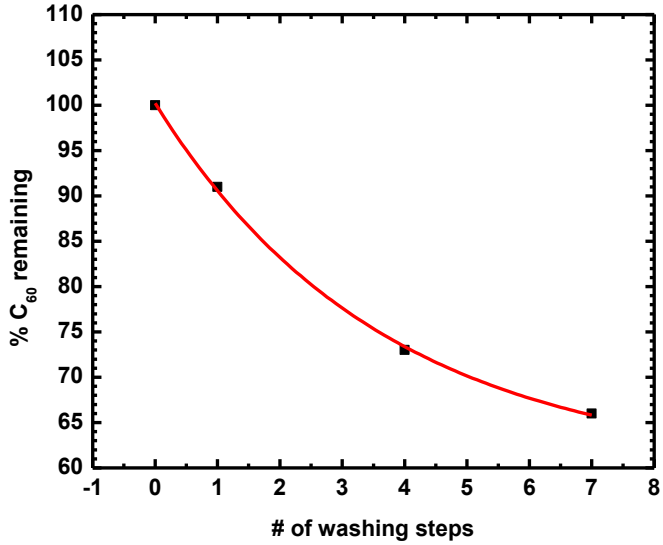

Figure 6.4 Plot of number of washing steps versus % C_{60} remaining in the film

Additionally, the 336 nm peak in UV/Vis absorbance spectra of the toluene washings was identical to that expected for absorption maximum of pristine, underivatized C_{60} in toluene.[97] Hence, it was indicated that there no transformations or derivatization on the C_{60} molecules occurred during synthesis. This was also evident from the characteristic purple color of the toluene washings which was due to individual C_{60} molecules. To further investigate the state of

C_{60} in DMF, high performance liquid chromatographic (HPLC) data were collected for C_{60}/DMF mixture. The resulted HPLC data and a chromatogram with the characteristic retention time for pristine, underivatized C_{60} dissolved in toluene using the same "CosmosilBuckyprep" packed column, are presented in Figure 6.5.

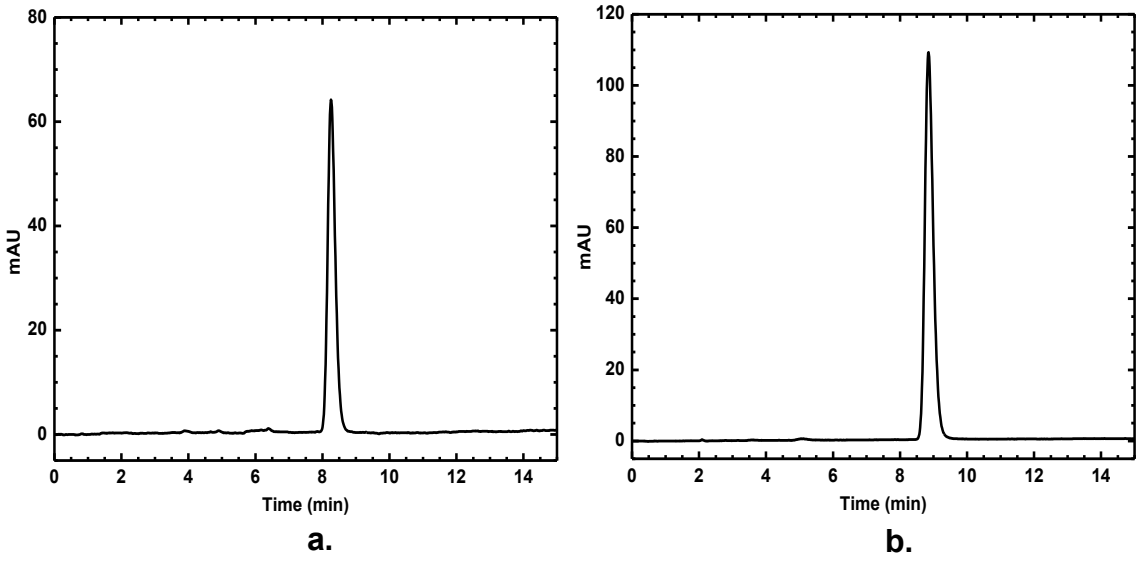

Figure 6.5 HPLC chromatograms showing, a) C_{60} in DMF and b) C_{60} in toluene

In both chromatograms the retention times and the peak shapes are almost identical except for the peak intensities which occurred due to different C_{60} concentrations used. This observation, along with the absorption maximum of 336 nm as measured by HPLC's photodiode array detector, further confirmed that C_{60} was not derivatized during the synthesis.

To investigate selective incorporation to the cyclodextrim pocket versus non-selective adsorption in the swelled network, new networks were made using α-CD and dibromododecane.

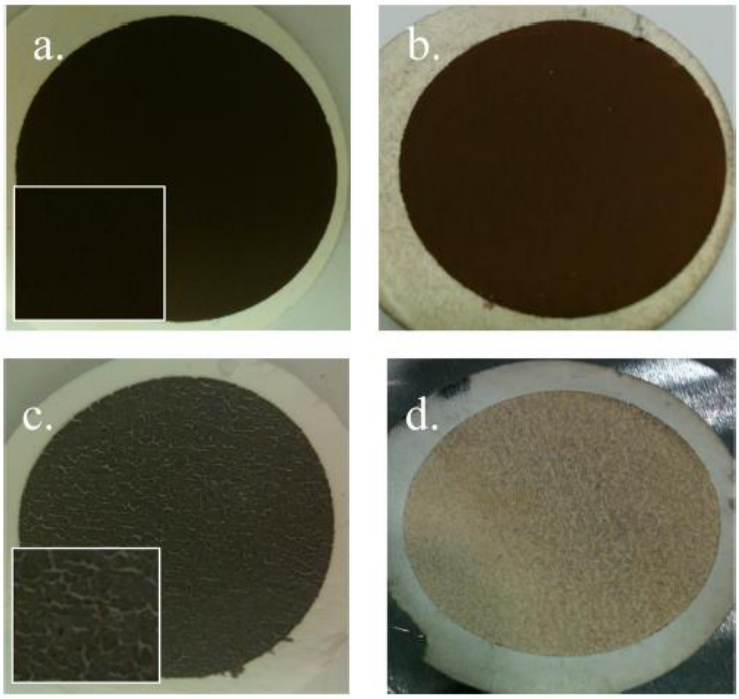

Figure 6.6 Comparison of as-prepared dry membranes versus membranes after washing in excess toluene for 1 h: (a) γ-CD/dodecyl/C_{60} membrane before wash; (b) same membrane as in (a) after toluene wash; (c) α-CD/dodecyl/C_{60} membrane before wash; (d) same membrane as in (c) after toluene wash. The insets in the lower left of (a) and (c) are 10× zoomed images[95]

As evident from the Figures 6.6a-d, in contrast to γ-CD/dodecyl networks, α-CD/dodecyl networks weren't capable of encapsulating C_{60} due to its smaller inner cavity size of about 0.57 nm in diameter (van der Waals dimension of large toroid end) which is significantly smaller than 1.0 nm van der Waals diameter of C_{60} or its atom-to-atom distance of 0.7 nm. As shown in Figure 6.6c the "as prepared" dry membrane of α-CD/dodecyl/C_{60} had a rough texture, and the dark color resulted from C_{60} distribution was not uniform as compared to the γ-CD/dodecyl/C_{60} membrane. Moreover in α-CD/dodecyl/C_{60} membrane almost all the C_{60} has been washed out after 1 hour wash with toluene, suggesting that no encapsulation occurred during the synthesis as expected due to the differences in inner cavity size of the host cyclodextrin molecule and the size of the

guest C_{60}. In comparison, the γ-CD/dodecyl/C_{60} membrane had retained two-thirds of the initial C_{60} even after five more consecutive toluene washes. All together this data confirmed that the γ-CD/dodecyl networks incorporate strongly bound C_{60}.

In these membranes it was not clear whether single-coordinate or bicoordinate C_{60}/CD complexes form, but earlier reports on C_{60}/CD coordination in solution phase has shown the tendency to form bicaapped complexes with γ-cyclodextrin.[98, 99]

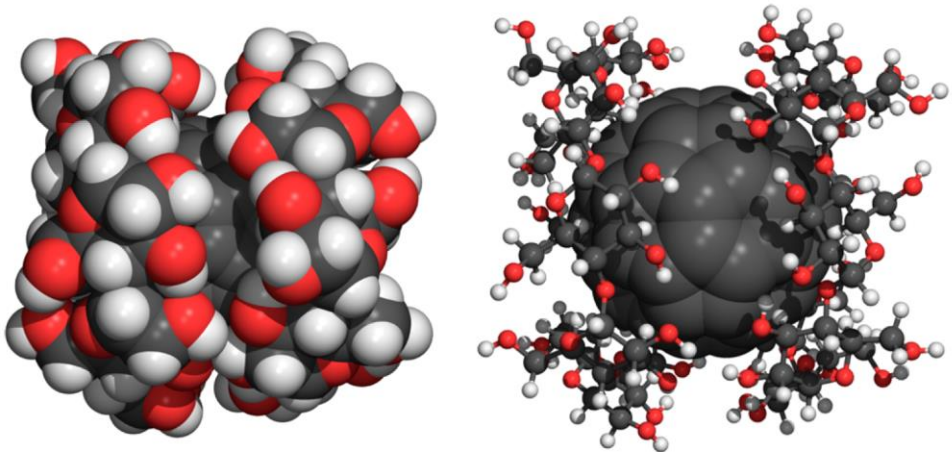

Figure 6.7 Scheme 1 CPK (left) and Partial Ball-and-Stick (right), structures of C_{60} and γ-Cyclodextrin complexes in solution, calculated via Geometry Optimization Using the MM+ Molecular Mechanics Potential in HyperChem 7

The MM+ molecular mechanics calculations done for an energy-minimized structure of C_{60} and γ-CD, followed by modifying a method described by Seridi for the interactions of C_{60} and β-CD,[100] along with literature data, suggested that C_{60} can stabilize network formation and integrity through bicoordinate or bicapping associations with CD's. Calculated bicoordinate CD/C_{60} complexes are shown in Figure 6.7. We expected that this type of bicoordination could occur in the membrane areas where tie chain densities were low, but we do not expect all C_{60} to be bicapped by CD molecules. This conclusion of bicoordination can be further verified by the structural integrity and toughness resulted in the C_{60} intercalated membranes due to C_{60} acting as

a very robust, non-covalent linker compared to the membranes without $C_{60,}$ as shown in Figures 6.1 and 6.2.

6.4 Conclusions

A simple route for the synthesis of C_{60} intercalated γ-CD/dibromododecane network composite membranes was developed. The membranes were capable of sequestering 66% of C_{60} from the original amount added during the synthesis and demonstrated stable and homogenous C_{60} intercalation, and moreover, C_{60} was shown to act as a very robust non-covalent linker. Sequestered C_{60} molecules were found to be un-derivatized. Inner cavity size of cyclodextrin molecules and the tie chain length of the linkers were found to be variable parameters that affected intercalation efficiency of the networks.

CHAPTER VII

CONCLUTIONS AND FUTURE DIRECTIONS

Stable aqueous suspensions of colloidal C_{60}, termed nC_{60}, are poorly-understood[30] complex systems. Subtle effects from their specific synthetic preparations and surface chemistry dominate its stability and reactivity. Substantial data have been presented in the literature providing conflicting interpretations of this material's health and environmental implications and cytotoxicity.[11, 16, 34, 35, 37-40, 43, 47, 76-80] Most strikingly, the oxidative behavior of these colloidal aggregates remains only partially explained. Therefore, ascertaining which attributes of fullerene colloidal suspensions drive the observed oxidative responses, as well as identifying the mechanisms underlying any observed oxidation, is of vital importance. The work reported here develops a robust methodology for investigating the oxidative behavior of AQU/nC_{60} colloidal suspensions using probe-assisted spectroscopic determinations such as fluorescence spectroscopy and sophisticated kinetic data analysis techniques to elucidate mechanistic information. The present study successfully demonstrated that AQU/nC_{60} suspensions are indeed acting as oxidants, and the rate of oxidation was directly related to the concentration of nC_{60} present in the suspensions. Additionally a reliable method to measure oxidation in these or similar systems has been developed along with arbitrary kinetic models that showed

reproducibility and high precision in fitting kinetic data. Although the present study clarified some questions related to observed oxidation, there is much yet to be explained such as developing and validating a kinetic model that uniformly fits the available data across all data sets. Moreover, the lipophilic nature of the probe molecule (rhodamine 123) might make the adsorption/desorption to the colloid surface important steps to consider in the ultimate kinetic mechanism.

Initial attempts to investigate the thermal stability of these colloidal suspensions revealed that AQU/*n*C_{60} suspensions were stable up to 98-100°C. Further experimentation on AQU/*n*C_{60} confirmed that there was no measurable thermally activated transformation occurring during heating, which disproved our initial hypothesis of the formation of $C_{120}O$. Further experimentation needs to be done using higher concentrations and other *n*C_{60} synthesis methods to verify the conclusion drawn in this initial work.

Additionally improvements were made to a quantification procedure of C_{60} in colloidal suspensions, and new procedures were established for this determination. While the previous UV/Vis spectroscopic method to quantify C_{60} was not sufficient to account for all variables, the new method developed using an HPLC calibration curve method showed significant improvements in this determination.

Finally, a novel architecture using guest-host properties of γ-cyclodextrin and C_{60} has been successfully developed which may open new synthesis routes for polymer composite networks. A simple route for the incorporating C_{60} into a γ-CD/dibromododecane network composite membranes was presented in this study, which

demonstrated stable and homogenous C_{60} incorporation where C_{60} was shown to act as a robust non-covalent linker. Moreover the novel architectural composite presented in this study might be of potential interest to applications such as sequestration of C_{60} to address environmental health and safety issues of this material.

REFERENCES

1. Osawa, E., *Kagaku* **1970**, 25, 854.

2. Davidson, R. A., Unified Theory of Graph Spectral Reduction Networks .4. Spectral-Analysis of Graphs by Cyclic Automorphism Subgroups. *Theor Chim Acta* **1981**, 58, 193-231.

3. Haymet, A. D. J., C120 and C60: Archimedean Solids Constructed from Sp2 Hybridized Carbon Atoms. *Chemical Physics Letters* **1985**, 122, 421-424.

4. Kroto, H. W.; Heath, J. R.; O'Brien, S. C.; Curl, R. F.; Smalley, R. E., C60: Buckminsterfullerene. *Nature* **1985**, 318, 162-163.

5. Smalley, R. E., Discovering the Fullerenes. *Reviews of Modern Physics* **1997**, 69, 723-730.

6. Kratschmer, W.; Lamb, L. D.; Fostiropoulos, K.; Huffman, D. R., Solid C-60 - a New Form of Carbon. *Nature* **1990**, 347, 354-358.

7. Murayama, H.; Tomonoh, S.; Alford, J. M.; Karpuk, M. E., Fullerene Production in Tons and More: From Science to Industry. *Fuller Nanotub Car N* **2004**, 12, 1-9.

8. Korobov, M. V.; Smith, A. L., Fullerenes: Chemistry, Physics and Technology *John Wiley and Sons, Inc.* **2000**.

9. Andrievsky, G. V.; Kosevich, M. V.; Vovk, O. M.; Shelkovsky, V. S.; Vashchenko, L. A., On the Production of an Aqueous Colloidal Solution of Fullerenes. *J Chem Soc Chem Comm* **1995**, 1281-1282.

10. Labille, J.; Brant, J.; Villieras, F.; Pelletier, M.; Thill, A.; Masion, A.; Wiesner, M.; Rose, J.; Bottero, J. Y., Affinity of C-60 Fullerenes with Water. *Fuller Nanotub Car N* **2006**, 14, 307-314.

11. Fortner, J. D.; Lyon, D. Y.; Sayes, C. M.; Boyd, A. M.; Falkner, J. C.; Hotze, E. M.; Alemany, L. B.; Tao, Y. J.; Guo, W.; Ausman, K. D.; Colvin, V. L.; Hughes, J. B., C60 in Water: Nanocrystal Formation and Microbial Response. *Environ. Sci. Technol.* **2005**, 39, 4307-4316.

12. Brant, J. A.; Labille, J.; Bottero, J. Y.; Wiesner, M. R., Characterizing the Impact of Preparation Method on Fullerene Cluster Structure and Chemistry. *Langmuir* **2006**, 22, 3878-3885.

13. Scrivens, W. A.; Tour, J. M.; Creek, K. E.; Pirisi, L., Synthesis of C-14-Labeled C-60, Its Suspension in Water, and Its Uptake by Human Keratinocytes. *J Am Chem Soc* **1994**, 116, 4517-4518.

14. Hilburn, M. E.; Murdianti, B. S.; Maples, R. D.; Williams, J. S.; Damron, J. T.; Kuriyavar, S. I.; Ausman, K. D., Synthesizing Aqueous Fullerene Colloidal Suspensions by New Solvent-Exchange Methods. *Colloid Surface A* **2012**, 401, 48-53.

15. Deguchi, S.; Alargova, R. G.; Tsujii, K., Stable Dispersions of Fullerenes, C-60 and C-70, in Water. Preparation and Characterization. *Langmuir* **2001**, 17, 6013-6017.

16. Sayes, C. M.; Fortner, J. D.; Guo, W.; Lyon, D.; Boyd, A. M.; Ausman, K. D.; Tao, Y. J.; Sitharaman, B.; Wilson, L. J.; Hughes, J. B.; West, J. L.; Colvin, V. L., The Differential Cytotoxicity of Water-Soluble Fullerenes. *Nano Lett* **2004**, 4, 1881-1887.

17. Eastoe, J.; Crooks, E. R.; Beeby, A.; Heenan, R. K., Structure and Photophysics in C-60-Micellar Solutions. *Chemical Physics Letters* **1995**, 245, 571-577.

18. Mohan, H.; Palit, D. K.; Chiang, L. Y.; Mittal, J. P., Radiation Chemical and Photophysical Properties of C-60(C4h8so3na)(N) in Aqueous Solution: A Laser Flash Photolysis and Pulse Radiolysis Study. *Fullerene Sci Techn* **2001**, 9, 37-53.

19. Wharton, T.; Kini, V. U.; Mortis, R. A.; Wilson, L. J., New Non-Ionic, Highly Water-Soluble Derivatives of C-60 Designed for Biological Compatibility. *Tetrahedron Lett* **2001**, 42, 5159-5162.

20. Samal, S.; Choi, B. J.; Geckeler, K. E., The First Water-Soluble Main-Chain Polyfullerene. *Chem Commun* **2000**, 1373-1374.

21. Reed, C. A.; Bolskar, R. D., Discrete Fulleride Anions and Fullerenium Cations. *Chemical reviews* **2000**, 100, 1075-120.

22. Cusan, C.; Da Ros, T.; Spalluto, G.; Foley, S.; Janto, J. M.; Seta, P.; Larroque, C.; Tomasini, M. C.; Antonelli, T.; Ferraro, L.; Prato, M., A New Multi-Charged C-60 Derivative: Synthesis and Biological Properties. *Eur J Org Chem* **2002**, 2928-2934.

23. Chiang, L. Y.; Swirczewski, J. W.; Hsu, C. S.; Chowdhury, S. K.; Cameron, S.; Creegan, K., Multi-Hydroxy Additions onto C60 Fullerene Molecules. *Journal of the Chemical Society, Chemical Communications* **1992**, 1791-1793.

24. Torres, V. M.; Posa, M.; Srdjenovic, B.; Simplício, A. L., Solubilization of Fullerene C60 in Micellar Solutions of Different Solubilizers. *Colloids and Surfaces B: Biointerfaces* **2011**, 82, 46-53.

25. Chen, K. L.; Smith, B. A.; Ball, W. P.; Fairbrother, D. H., Assessing the Colloidal Properties of Engineered Nanoparticles in Water: Case Studies from Fullerene C-60 Nanoparticles and Carbon Nanotubes. *Environ Chem* **2010**, 7, 10-27.

26. Mchedlov-Petrossyan, N. O.; Klochkov, V. K.; Andrievsky, G. V., Colloidal Dispersions of Fullerene C-60 in Water: Some Properties and Regularities of Coagulation by Electrolytes. *J Chem Soc Faraday T* **1997**, 93, 4343-4346.

27. Brant, J.; Lecoanet, H.; Wiesner, M., Aggregation and Deposition Characteristics of Fullerene Nanoparticles in Aqueous Systems. *J Nanopart Res* **2005**, 7, 545-553.

28. Brant, J.; Lecoanet, H.; Hotze, M.; Wiesner, M., Comparison of Electrokinetic Properties of Colloidal Fullerenes (N-C-60) Formed Using Two Procedures. *Environ Sci Technol* **2005**, 39, 6343-6351.

29. Alargova, R. G.; Deguchi, S.; Tsujii, K., Stable Colloidal Dispersions of Fullerenes in Polar Organic Solvents. *J Am Chem Soc* **2001**, 123, 10460-10467.

30. Labille, J.; Masion, A.; Ziarelli, F.; Rose, J.; Brant, J.; Villieras, F.; Pelletier, M.; Borschneck, D.; Wiesner, M. R.; Bottero, J. Y., Hydration and Dispersion of C-60 in Aqueous Systems: The Nature of Water-Fullerene Interactions. *Langmuir* **2009**, 25, 11232-11235.

31. Murdianti, B. S.; Damron, J. T.; Hilburn, M. E.; Maples, R. D.; Hikkaduwa Koralege, R. S.; Kuriyavar, S. I.; Ausman, K. D., C60 Oxide as a Key Component of Aqueous C60 Colloidal Suspensions. *Environ Sci Technol* **2012**, 46, 7446-7453.

32. Weisman, R. B.; Heymann, D.; Bachilo, S. M., Synthesis and Characterization of the "Missing" Oxide of C(60): [5,6]-Open C(60)O. *J Am Chem Soc* **2001**, 123, 9720-1.

33. Heymann, D.; Weisman, R. B., Fullerene Oxides and Ozonides. *Cr Chim* **2006**, 9, 1107-1116.

34. Sayes, C. M.; Gobin, A. M.; Ausman, K. D.; Mendez, J.; West, J. L.; Colvin, V. L., Nano-C-60 Cytotoxicity Is Due to Lipid Peroxidation. *Biomaterials* **2005**, 26, 7587-7595.

35. Oberdorster, E., Manufactured Nanomaterials (Fullerenes, C-60) Induce Oxidative Stress in the Brain of Juvenile Largemouth Bass. *Environ Health Persp* **2004**, 112, 1058-1062.

36. Isakovic, A.; Markovic, Z.; Todorovic-Markovic, B.; Nikolic, N.; Vranjes-Djuric, S.; Mirkovic, M.; Dramicanin, M.; Harhaji, L.; Raicevic, N.; Nikolic, Z.; Trajkovic, V., Distinct Cytotoxic Mechanisms of Pristine Versus Hydroxylated Fullerene. *Toxicol Sci* **2006**, 91, 173-183.

37. Lyon, D. Y.; Brunet, L.; Hinkal, G. W.; Wiesner, M. R.; Alvarez, P. J. J., Antibacterial Activity of Fullerene Water Suspensions (Nc(60)) Is Not Due to Ros-Mediated Damage. *Nano Lett* **2008**, 8, 1539-1543.

38. Andrievsky, G.; Klochkov, V.; Derevyanchenko, L., Is the C-60 Fullerene Molecule Toxic?! *Fuller Nanotub Car N* **2005**, 13, 363-376.

39. Gharbi, N.; Pressac, M.; Hadchouel, M.; Szwarc, H.; Wilson, S. R.; Moussa, F., [60]Fullerene Is a Powerful Antioxidant in Vivo with No Acute or Subacute Toxicity. *Nano Lett* **2005**, 5, 2578-2585.

40. Zhu, S. Q.; Oberdorster, E.; Haasch, M. L., Toxicity of an Engineered Nanoparticle (Fullerene, C-60) in Two Aquatic Species, Daphnia and Fathead Minnow. *Mar Environ Res* **2006**, 62, S5-S9.

41. Isakovic, A.; Markovic, Z.; Nikolic, N.; Todorovic-Markovic, B.; Vranjes-Djuric, S.; Harhaji, L.; Raicevi, N.; Romcevic, N.; Vasiljevic-Radovic, D.; Dramicanin, M.; Trajkovic, V., Inactivation of Nanocrystalline C-60 Cytotoxicity by Gamma-Irradiation. *Biomaterials* **2006**, 27, 5049-5058.

42. Wang, I. C.; Tai, L. A.; Lee, D. D.; Kanakamma, P. P.; Shen, C. K. F.; Luh, T.-Y.; Cheng, C. H.; Hwang, K. C., C60 and Water-Soluble Fullerene Derivatives as Antioxidants against Radical-Initiated Lipid Peroxidation. *Journal of Medicinal Chemistry* **1999**, 42, 4614-4620.

43. Zhu, X. S.; Zhu, L.; Lang, Y. P.; Chen, Y. S., Oxidative Stress and Growth Inhibition in the Freshwater Fish Carassius Auratus Induced by Chronic Exposure to Sublethal Fullerene Aggregates. *Environ Toxicol Chem* **2008**, 27, 1979-1985.

44. Henry, T. B.; Menn, F. M.; Fleming, J. T.; Wilgus, J.; Compton, R. N.; Sayler, G. S., Attributing Effects of Aqueous C-60 Nano-Aggregates to Tetrahydrofuran Decomposition Products in Larval Zebrafish by Assessment of Gene Expression. *Environ Health Persp* **2007**, 115, 1059-1065.

45. Kovochich, M.; Espinasse, B.; Auffan, M.; Hotze, E. M.; Wessel, L.; Xia, T.; Nel, A. E.; Wiesner, M. R., Comparative Toxicity of C-60 Aggregates toward Mammalian Cells: Role of Tetrahydrofuran (Thf) Decomposition. *Environ Sci Technol* **2009**, 43, 6378-6384.

46. Lovern, S. B.; Klaper, R., Daphnia Magna Mortality When Exposed to Titanium Dioxide and Fullerene (C-60) Nanoparticles. *Environ Toxicol Chem* **2006**, 25, 1132-1137.

47. Spohn, P.; Hirsch, C.; Hasler, F.; Bruinink, A.; Krug, H. F.; Wick, P., C60 Fullerene: A Powerful Antioxidant or a Damaging Agent? The Importance of an in-Depth Material Characterization Prior to Toxicity Assays. *Environ Pollut* **2009**, 157, 1134-9.

48. Robertson, A., Tetrahydrofuran Hydroperoxide. *Nature* **1948**, 162, 153-153.

49. Shurvell, H. F.; Southby, M. C., Infrared and Raman Spectra of Tetrahydrofuran Hydroperoxide. *Vib Spectrosc* **1997**, 15, 137-146.

50. Ma, C. C. M.; Sung, S. C.; Wang, F. Y.; Chiang, L. Y.; Wang, L. Y.; Chiang, C. L., Thermal, Mechanical, and Morphological Properties of Novolac-Type Phenolic Resin Blended with Fullerenol Polyurethane and Linear Polyurethane. *J Polym Sci Pol Phys* **2001**, 39, 2436-2443.

51. Wang, M.; Pramoda, K. P.; Goh, S. H., Mechanical Behavior of Pseudo-Semi-Interpenetrating Polymer Networks Based on Double-C-60-End-Capped Poly(Ethylene Oxide) and Poly(Methyl Methacrylate). *Chem Mater* **2004**, 16, 3452-3456.

52. Kai, W. H.; Zhao, L.; Zhu, B.; Inoue, Y., Mechanical Properties of Blends of Double-Fullerene End-Capped Poly(Ethylene Oxide) and Poly(L-Lactic Acid). *Macromol Chem Physic* **2006**, 207, 746-754.

53. Olkhov, Y. A.; Jurkowski, B., Effect of Fullerenes on the Structure and Properties of Linear and Crosslinked Polyesterurethane Ureas. *J Appl Polym Sci* **2007**, 104, 1431-1442.

54. Liang, Y.; Yu, L., A New Class of Semiconducting Polymers for Bulk Heterojunction Solar Cells with Exceptionally High Performance. *Accounts of chemical research* **2010**, 43, 1227-36.

55. Liu, W. L.; Liu, R. G.; Wang, W.; Li, W. W.; Liu, W. Y.; Zheng, K.; Ma, L.; Tian, Y.; Bo, Z. S.; Huang, Y., Tailoring Nanowire Network Morphology and Charge Carrier Mobility of Poly(3-Hexylthiophene)/C-60 Films. *J Phys Chem C* **2009**, 113, 11385-11389.

56. Liu, B.; Png, R. Q.; Zhao, L. H.; Chua, L. L.; Friend, R. H.; Ho, P. K. H., High Internal Quantum Efficiency in Fullerene Solar Cells Based on Crosslinked Polymer Donor Networks. *Nat Commun* **2012**, 3.

57. Alem, S.; de Bettignies, R.; Nunzi, J. M.; Cariou, M., Efficient Polymer-Based Interpenetrated Network Photovoltaic Cells. *Appl Phys Lett* **2004**, 84, 2178-2180.

58. Gebeyehu, D.; Padinger, F.; Brabec, C. J.; Fromherz, T.; Hummelen, J. C.; Sariciftci, N. S., Characterization of Large Area Flexible Plastic Solar Cells Based on Conjugated Polymer/Fullerene Composites. *Int J Photoenergy* **1999**, 1.

59. Biryulin, Y. F.; Zgonnik, V. N.; Melenevskaya, E. Y.; Mikov, S. N.; Moliver, S. S.; Orlov, S. E.; Novoselova, A. V.; Petrikov, V. D.; Rozanov, V. V.; Sykmanov, D. A.; Yagovkina, M. A., Structure and Optical Properties of C-60 Films on Polymer Substrates. *Semiconductors+* **2003**, 37, 347-353.

60. Andersson, T.; Nilsson, K.; Sundahl, M.; Westman, G.; Wennerstrom, O., C60 Embedded in [Gamma]-Cyclodextrin: A Water-Soluble Fullerene. *Journal of the Chemical Society, Chemical Communications* **1992**, 604-606.

61. Raffaini, G.; Ganazzoli, F., A Molecular Dynamics Study of the Inclusion Complexes of C60 with Some Cyclodextrins. *The Journal of Physical Chemistry B* **2010**, 114, 7133-7139.

62. van de Manakker, F.; Vermonden, T.; van Nostrum, C. F.; Hennink, W. E., Cyclodextrin-Based Polymeric Materials: Synthesis, Properties, and Pharmaceutical/Biomedical Applications. *Biomacromolecules* **2009**, 10, 3157-3175.

63. Del Valle, E. M. M., Cyclodextrins and Their Uses: A Review. *Process Biochemistry* **2004**, 39, 1033-1046.

64. Fenyvesi, É.; Ujházy, A.; Szejtli, J.; Potter, S.; Gan, T. G., Controlled Release of Drugs from Cd Polymers Substituted with Ionic Groups. *J Incl Phenom Macrocycl Chem* **1996**, 25, 185-189.

65. Rodriguez-Tenreiro, C.; Alvarez-Lorenzo, C.; Rodriguez-Perez, A.; Concheiro, A.; Torres-Labandeira, J. J., Estradiol Sustained Release from High Affinity Cyclodextrin Hydrogels. *European Journal of Pharmaceutics and Biopharmaceutics* **2007**, 66, 55-62.

66. Rodriguez-Tenreiro, C.; Alvarez-Lorenzo, C.; Rodriguez-Perez, A.; Concheiro, A.; Torres-Labandeira, J., New Cyclodextrin Hydrogels Cross-Linked with Diglycidylethers

with a High Drug Loading and Controlled Release Ability. *Pharm Res* **2006**, 23, 121-130.

67. Gyanwali, G.; Hodge, M.; White, J. L., Cyclodextrin Functionalization: Simple Routes to Tailored Solubilities and Nanoscopic Polymer Networks. *Journal of Polymer Science Part A: Polymer Chemistry* **2012**, 50, 3269-3276.

68. Gyanwali, G.; Hodge, M.; White, J. L., Orthogonal Polymer Networks That Contain Dynamic Nodes. *Polymer* **2013**, 54, 2257-2263.

69. Lebedkin, S.; Ballenweg, S.; Gross, J.; Taylor, R.; Kratschmer, W., Synthesis of C120o - a New Dimeric [60]Fullerene Derivative. *Tetrahedron Lett* **1995**, 36, 4971-4974.

70. Smith, A. B.; Tokuyama, H.; Strongin, R. M.; Furst, G. T.; Romanow, W. J.; Chait, B. T.; Mirza, U. A.; Haller, I., Synthesis of Oxo-Bridged and Methylene-Bridged C-60 Dimers, the First Well-Characterized Species Containing Fullerene-Fullerene Bonds. *J Am Chem Soc* **1995**, 117, 9359-9360.

71. Chibante, L. P. F.; Heymann, D., On the Geochemistry of Fullerenes - Stability of C-60 in Ambient Air and the Role of Ozone. *Geochim Cosmochim Ac* **1993**, 57, 1879-1881.

72. Amer, M. S.; Abdu, M. T., On the Evaporation Kinetics of C60/Toluene Solutions. *Philosophical Magazine Letters* **2009**, 89, 615-621.

73. Colvin, V. L., The Potential Environmental Impact of Engineered Nanomaterials. *Nat Biotech* **2003**, 21, 1166-1170.

74. Johnston, H. J.; Hutchison, G. R.; Christensen, F. M.; Aschberger, K.; Stone, V., The Biological Mechanisms and Physicochemical Characteristics Responsible for Driving Fullerene Toxicity. *Toxicol Sci* **2010**, 114, 162-182.

75. Aschberger, K.; Johnston, H. J.; Stone, V.; Aitken, R. J.; Tran, C. L.; Hankin, S. M.; Peters, S. A. K.; Christensen, F. M., Review of Fullerene Toxicity and Exposure – Appraisal of a Human Health Risk Assessment, Based on Open Literature. *Regulatory Toxicology and Pharmacology* **2010**, 58, 455-473.

76. Dhawan, A.; Taurozzi, J. S.; Pandey, A. K.; Shan, W. Q.; Miller, S. M.; Hashsham, S. A.; Tarabara, V. V., Stable Colloidal Dispersions of C-60 Fullerenes in Water: Evidence for Genotoxicity. *Environ Sci Technol* **2006**, 40, 7394-7401.

77. Lyon, D. Y.; Alvarez, P. J., Fullerene Water Suspension (Nc60) Exerts Antibacterial Effects Via Ros-Independent Protein Oxidation. *Environ Sci Technol* **2008**, 42, 8127-32.

78. Levi, N.; Hantgan, R. R.; Lively, M. O.; Carroll, D. L.; Prasad, G. L., C60-Fullerenes: Detection of Intracellular Photoluminescence and Lack of Cytotoxic Effects. *Journal of nanobiotechnology* **2006**, 4, 14.

79. Shinohara, N.; Matsumoto, T.; Gamo, M.; Miyauchi, A.; Endo, S.; Yonezawa, Y.; Nakanishi, J., Is Lipid Peroxidation Induced by the Aqueous Suspension of Fullerene C-60 Nanoparticles in the Brains of Cyprinus Carpio? *Environ Sci Technol* **2009**, 43, 948-953.

80. Oberdorster, E.; Zhu, S. Q.; Blickley, T. M.; McClellan-Green, P.; Haasch, M. L., Ecotoxicology of Carbon-Based Engineered Nanoparticles: Effects of Fullerene (C-60) on Aquatic Organisms. *Carbon* **2006**, 44, 1112-1120.

81. Bartosz, G., Use of Spectroscopic Probes for Detection of Reactive Oxygen Species. *Clin Chim Acta* **2006**, 368, 53-76.

82. Soh, N., Recent Advances in Fluorescent Probes for the Detection of Reactive Oxygen Species. *Anal Bioanal Chem* **2006**, 386, 532-543.

83. Gomes, A.; Fernandes, E.; Lima, J. L. F. C., Fluorescence Probes Used for Detection of Reactive Oxygen Species. *J Biochem Bioph Meth* **2005**, 65, 45-80.

84. Rothe, G.; Oser, A.; Valet, G., Dihydrorhodamine-123 - a New Flow Cytometric Indicator for Respiratory Burst Activity in Neutrophil Granulocytes. *Naturwissenschaften* **1988**, 75, 354-355.

85. Miranda, K. M.; Espey, M. G.; Yamada, K.; Krishna, M.; Ludwick, N.; Kim, S.; Jourd'heuil, D.; Grisham, M. B.; Feelisch, M.; Fukuto, J. M.; Wink, D. A., Unique Oxidative Mechanisms for the Reactive Nitrogen Oxide Species, Nitroxyl Anion. *The Journal of biological chemistry* **2001**, 276, 1720-7.

86. Steinfeld, J. I.; Francisco, J. S.; Hase, W. L., *Chemical Kinetics and Dynamics*. 2nd Edition ed.; Prentice Hall: 1998.

87. Taylor, R.; Barrow, M. P.; Drewello, T., C-60 Degrades to C120o. *Chem Commun* **1998**, 2497-2498.

88. Paul, P.; Kim, K. C.; Sun, D. Y.; Boyd, P. D. W.; Reed, C. A., Artifacts in the Electron Paramagnetic Resonance Spectra of C-60 Fullerene Ions: Inevitable C120o Impurity. *J Am Chem Soc* **2002**, 124, 4394-4401.

89. Maples, R. D.; Hilburn, M. E.; Murdianti, B. S.; Koralege, R. S. H.; Williams, J. S.; Kuriyavar, S. I.; Ausman, K. D., Optimized Solvent-Exchange Synthesis Method for C-60 Colloidal Dispersions. *J Colloid Interf Sci* **2012**, 370, 27-31.

90. Andrievsky, G. V.; Klochkov, V. K.; Bordyuh, A. B.; Dovbeshko, G. I., Comparative Analysis of Two Aqueous-Colloidal Solutions of C-60 Fullerene with Help of Ftir Reflectance and Uv-Vis Spectroscopy. *Chemical Physics Letters* **2002**, 364, 8-17.

91. Xie, B.; Xu, Z. H.; Guo, W. H.; Li, Q. L., Impact of Natural Organic Matter on the Physicochemical Properties of Aqueous C-60 Nanoparticles. *Environ Sci Technol* **2008**, 42, 2853-2859.

92. Duncan, L. K.; Jinschek, J. R.; Vikesland, P. J., C60 Colloid Formation in Aqueous Systems: Effects of Preparation Method on Size, Structure, and Surface Charge. *Environ Sci Technol* **2008**, 42, 173-8.

93. Zhang, W.; Gong, X.; Liu, C.; Piao, Y.; Sun, Y.; Diao, G., Water-Soluble Inclusion Complex of Fullerene with [Gamma]-Cyclodextrin Polymer for Photodynamic Therapy. *Journal of Materials Chemistry B* **2014**, 2, 5107-5115.

94. Braun, T.; Buvári-Barcza, Á.; Barcza, L.; Konkoly-Thege, I.; Fodor, M.; Migali, B., Mechanochemistry: A Novel Approach to the Synthesis of Fullerene Compounds. Water Soluble Buckminsterfullerene - Γ-Cyclodextrin Inclusion Complexes Via a Solid-Solid Reaction. *Solid State Ionics* **1994**, 74, 47-51.

95. Gyanwali, G.; Koralege, R. S. H.; Hodge, M.; Ausman, K. D.; White, J. L., C-60-Polymer Nanocomposite Networks Enabled by Guest Host Properties. *Macromolecules* **2013**, 46, 6118-6123.

96. Ruoff, R. S.; Tse, D. S.; Malhotra, R.; Lorents, D. C., Solubility of Fullerene (C60) in a Variety of Solvents. *The Journal of Physical Chemistry* **1993**, 97, 3379-3383.

97. Bachilo, S. M.; Benedetto, A. F.; Weisman, R. B., Triplet State Dissociation of C-120, the Dimer of C-60. *J Phys Chem B* **2001**, 105, 21a-22a.

98. Andersson, T.; Westman, G.; Wennerstrom, O.; Sundahl, M., Nmr and Uv-Vis Investigation of Water-Soluble Fullerene-60-[Gamma]-Cyclodextrin Complex. *Journal of the Chemical Society, Perkin Transactions 2* **1994**, 1097-1101.

99. Nishibayashi, Y.; Saito, M.; Uemura, S.; Takekuma, S.-i.; Takekuma, H.; Yoshida, Z.-i., Buckminsterfullerenes: A Non-Metal System for Nitrogen Fixation. *Nature* **2004**, 428, 279-280.

100. Seridi, L.; Boufelfel, A., Simulations of Docking C60 in B-Cyclodextrin. *Journal of Molecular Liquids* **2011**, 162, 69-77.

VITA

Rangika S. Hikkaduwa Koralege

Candidate for the Degree of

Doctor of Philosophy

Thesis: OXIDATIVE BEHAVIOR AND THERMAL STABILITY OF C_{60} COLLOIDAL SUSPENSIONS IN WATER AND GUEST-HOST INTERACTIONS OF C_{60}/γ-CYCLODEXTRIN POLYMER NETWORKS

Major Field: Chemistry

Biographical:

Education:
Completed the requirements for the Doctor of Philosophy in Chemistry at Oklahoma State University, Stillwater, Oklahoma, in December, 2014.

Completed the requirements for the Bachelor of Science in Chemistry at University of Kelaniya, Kelaniya, Sri Lanka, in 2007.

Personal Data: Born in Minuwangoda City, Sri Lanka, on March, 21st, 1981, as the daughter of Hikkaduwa Koralege Victor and Bopagoda Hettige Nandawathie.

Experience: Teaching/Research Assistant, Depertment of Chemistry, Oklahoma State University (January 2010-December 2014), Accreditation Officer, Sri Lanka Accreditation Board, Ministry of Science and Technology, Sri Lanka (June 2008-June 2009), Teaching Assistant, Department of Chemistry, University of Kelaniya, Sri Lanka (May 2007-March 2008), Research Assistant, Department of Chemistry, University of Kelaniya, Sri Lanka (May 2006-April 2007).

Professional Memberships: Phi Kappa Phi National Honor Society, Graduate and Professional Student Government Association, American Chemical Society.